Displaced Geostationary Orbit Design Using Hybrid Sail Propulsion

Jeannette Heiligers[*], Matteo Ceriotti[†], Colin R. McInnes[‡] and James D. Biggs[§]

University of Strathclyde, Glasgow G1 1XJ, Scotland, United Kingdom

Abstract

Due to an increase in number of geostationary spacecraft and limits imposed by east-west spacing requirements, the geostationary orbit is becoming congested. To increase its capacity, this paper proposes to create new geostationary slots by displacing the geostationary orbit either out of or in the equatorial plane by means of hybrid solar sail and solar electric propulsion. To minimize propellant consumption, optimal steering laws for the solar sail and solar electric propulsion thrust vectors are derived and the performance in terms of mission lifetime is assessed. For comparison, similar analyses are performed for conventional propulsion, including impulsive and pure solar electric propulsion. It is shown that hybrid sails outperform these propulsion techniques and that out-of-plane displacements outperform in-plane displacements. The out-of-plane case is therefore further investigated in a spacecraft mass budget to determine the payload mass capacity. Finally, two transfers that enable a further improvement of the performance of hybrid sails for the out-of-plane case are optimized using a direct pseudo-spectral method: a seasonally transit between orbits displaced above and below the equatorial plane and a transit to a parking orbit when geostationary coverage is not needed. Both transfers are shown to require only a modest propellant budget, outweighing the improvements they can establish.

---

[*] Ph.D. Candidate, Advanced Space Concepts Laboratory, Department of Mechanical Engineering

[†] Research Fellow, Advanced Space Concepts Laboratory, Department of Mechanical Engineering, AIAA Member

[‡] Director, Advanced Space Concepts Laboratory, Department of Mechanical Engineering, AIAA Member

[§] Associate Director, Advanced Space Concepts Laboratory, Department of Mechanical Engineering

Nomenclature

$\mathbf{a}$	Thrust induced acceleration vector
A	Area
c_1, c_2	Constants
g_0	Earth standard gravitational acceleration at surface , 9.80665m/s^2
h	Out-of-plane displacement distance
i_{obl}	Obliquity of the ecliptic
I_{sp}	Specific impulse
J	Cost function
k	Specific performance
L	Mission lifetime
m	Mass
m_{gimbal}	Gimbal mass
m_P	SEP thruster power source mass
m_{pay}	Payload mass
m_{prop}	Propellant mass
m_{tank}	SEP propellant tank mass
n	Integer
$\hat{\mathbf{n}}$	Solar sail acceleration unit vector
N	Number of impulses per orbit
P	Power
$\mathbf{r}$	Position vector
t	Time
$\mathbf{T}$	SEP thrust vector
t_p	Time in between impulses
$\mathbf{u}$	Control vector
U	Effective potential
V	Velocity

W	Solar energy flux density at 1 AU, 1367 W/m^2
$\mathbf{x}$	State vector
α	Pitch angle
β	Solar sail lightness number
γ	Sun incidence angle
δ	Yaw angle
Δd	Distance between spacecraft and GEO
Δm	Change in mass
Δr	In-plane displacement
Δt	Time interval
ΔV	Instantaneous velocity change
η	Efficiency
θ	In-plane angle (cylindrical/spherical coordinates)
μ	Gravitational parameter of central body
ρ	Projected orbital radius (cylindrical coordinates)
σ	System loading
σ^*	Critical sail loading, 1.53 g/m^2
τ	Orbital period
ϕ	Out-of-plane angle (spherical coordinates)
χ	Angle in Earth orbital plane measured from winter solstice
ψ	Angle between $\mathbf{r}_s$ and equatorial plane
$\boldsymbol{\omega}$	Angular velocity vector
ω_*	Orbital angular velocity of a circular Keplerian orbit with $r = r_{NKO}$

Subscripts

0	At time $t = t_0$
C	In Earth fixed inertial reference frame
E	In Earth fixed rotating reference frame

GEO	Referring to geostationary orbit
f	At final time
i	At i^{th} node
max	Maximum
min	Minimum
NKO	Referring to non-Keplerian orbit
r,θ,ϕ	Referring to spherical coordinate components
R	In rotating reference frame
s	Referring to solar sail
S	Referring to Sun
SA	Referring to solar array
SEP	Referring to solar electric propulsion
TF	Referring to thin film solar cells

Superscripts

-	Prior to impulsive ΔV
+	After impulsive ΔV
*	Optimal
$\dot{\square}$	First order derivative
$\ddot{\square}$	Second order derivative
$\hat{\square}$	Unit vector

Introduction

The geostationary orbit (GEO) hosts satellites for telecommunication and Earth observation. With an orbit period equal to the Earth's rotational period, spacecraft in GEO are stationary with respect to an observer on the Earth, allowing for a continuous downlink to terrestrial communications users. But, with only one such unique orbit, the GEO has become congested over time, especially above the continents where concentrations of geostationary satellites are greatest [1].

In order to create new geostationary slots, this paper investigates the use of displaced non-Keplerian orbits (NKOs) to displace the GEO either above/below or in the equatorial plane. Such displaced NKOs can be generated by applying a continuous, thrust-induced acceleration to counterbalance or augment part of the local gravitational acceleration [2]. The existence, stability and control of displaced NKOs have been studied for both the two- and three body problem [3-5] and numerous applications have been proposed. These applications range from spacecraft proximity operations [6] to NKOs displaced high above the ecliptic to enable imaging and communication for high latitudes [7] and displaced NKOs for lunar far side communication and lunar south pole coverage [8-9].

Solar sails have often been proposed as spacecraft propulsion system to maintain displaced NKOs [2, 4, 7-8, 10]. Solar sails exploit the radiation pressure generated by photons reflecting off a large, highly reflecting sail to produce a continuous, propellant-less thrust [2]. Although the concept of solar sailing has been considered for many years, only recently has a small sail been successfully deployed by the Japanese demonstrator mission IKAROS and by NASA's NanoSail-D nanosatellite [11-12]. Despite this advance, the Technology Readiness Level (TRL) of solar sailing as primary propulsion system on a reasonable sized mission is still rather low. That, in combination with a high advancement degree of difficulty [13] and the inability to generate a thrust component in the direction of the Sun [2] limits the applications of solar sailing.

Solar electric propulsion (SEP) has also been considered as a means to maintain displaced NKOs [9, 14]. SEP uses the acceleration of ions to produce a relatively low thrust, but enables high specific impulses. It has flown on multiple missions including Deep Space 1 (1998), SMART-1 (2003), Dawn (2007) and GOCE (2009), resulting in a high TRL and a low advancement degree of difficulty. Nevertheless, the applications of SEP are also limited due to a bound on the available propellant mass.

Considering the disadvantages and limitations of solar sails and SEP, some authors are suggesting to hybridize the two systems, because the separate systems complement each other: since only small solar sails will be required, the hybridization lowers the solar sail advancement degree of difficulty. Furthermore, while the solar sail lowers the demand on the SEP propellant mass, the SEP system can provide a thrust component in the direction of the Sun (which the solar sail is unable to generate). This is under the assumption that the SEP system is mounted on a gimbal such that the two propulsion systems can steer independently of each other. Hybrid sails have already been suggested to enable interplanetary transfers [15-16], to allow for periodic orbits in the vicinity of the Lagrange points in the Earth-Moon system for lunar communication purposes [17], and to generate artificial equilibria in the Earth-Sun

three-body problem [18-20]. All studies show to some extent an improvement for hybrid sails over the use of pure SEP or pure solar sailing in terms of propellant mass consumption, required thrust magnitude levels and/or initial spacecraft mass.

In this paper, we propose the use of hybrid sails to enable out-of-plane and in-plane displaced GEOs, thereby extending initial research conducted for out-of-plane displaced GEOs in Ref. [21]. Furthermore, compared to the solar sail levitated GEO proposed in Ref. [10] and [22], the displaced GEO proposed in this paper will allow spacecraft to be stationary with respect to their ground station, because the residual in-plane acceleration that causes a drift in the pure solar sail case can be cancelled by the SEP thruster. Also, displacements well beyond the geostationary station keeping box will be enabled using relatively small, near-term solar sails.

After a brief introduction in Section I of the general theory underlying two-body displaced NKOs using continuous control, the out-of-plane and in-plane displaced GEOs as investigated in this paper will be defined. Using these definitions, Sections II and III will derive the performance of impulsive and pure SEP control for maintaining the displaced GEO in terms of propellant consumption and mission lifetime. Similar results will be obtained for the hybrid sail case in Section IV by deriving the SEP and solar sail optimal steering laws. Since the out-of-plane case outperforms the in-plane case, the out-of-plane case will be used for a detailed mass budget analysis in Section V to assess the performance in terms of payload mass capacity. Finally, two types of transfer that improve the performance of the out-of-plane displaced GEO will be optimized for the SEP propellant consumption by solving the accompanying optimal control problem in Section VI and results in terms of SEP propellant mass will be presented.

I. Displaced GEOs

Displaced GEOs, or displaced NKOs in general, can be found by seeking equilibrium solutions to the two-body problem in a rotating frame of reference. A transformation to an inertial frame will subsequently show that the spacecraft executes a circular orbit displaced away from the nominal Keplerian orbit [3]. Fig. 1 shows these reference frames where $R(x_R, y_R, z_R)$ is a rotating frame of reference that rotates with constant angular velocity $\boldsymbol{\omega} = \omega \hat{\mathbf{z}}_R$ with respect to an inertial frame $I(X, Y, Z)$, where the z_R axis and Z axis coincide. Furthermore, to maintain the displaced NKO a thrust-induced acceleration $\mathbf{a}$ is assumed. The equations of motion of the spacecraft in the rotating reference frame are then given by:

$$\ddot{\mathbf{r}} + 2\boldsymbol{\omega} \times \dot{\mathbf{r}} + \nabla U = \mathbf{a} \tag{1}$$

with μ the gravitational parameter of the central body and U the effective potential that combines the gravitational potential of the central body and a potential that represents the centripetal acceleration:

$$U = -(\mu / r) - \frac{1}{2}\left\|\boldsymbol{\omega} \times \mathbf{r}\right\|^2 \tag{2}$$

Equilibrium solutions can subsequently be found by setting $\dot{\mathbf{r}} = \ddot{\mathbf{r}} = 0$ in Eq. (1), eliminating the first two terms:

$$\nabla U = \mathbf{a} \tag{3}$$

which directly gives the magnitude and direction of the thrust acceleration required to maintain the displaced NKO.

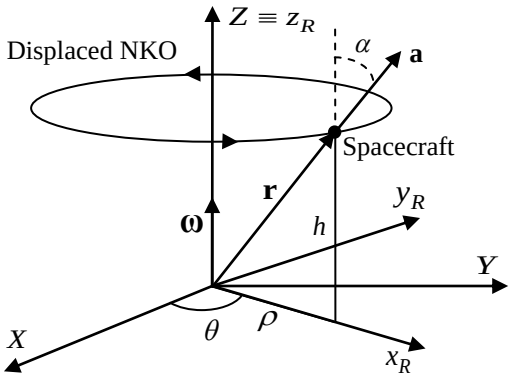

Fig. 1 Displaced non-Keplerian orbit reference frames.

Because $\boldsymbol{\omega}$ is constant, no transverse component of the thrust can exist, requiring the thrust vector to lie in the plane spanned by the radius vector and the vertical axis. The thrust direction is therefore defined by the pitch angle α only:

$$\tan\alpha = \frac{\left\|\hat{\mathbf{z}}_R \times \nabla U\right\|}{\hat{\mathbf{z}}_R \cdot \nabla U} \tag{4}$$

Finally, the potential U can be written using a set of cylindrical polar coordinates (ρ, θ, h) as shown in Fig. 1:

$$U = -\left(\frac{1}{2}(\omega\rho)^2 + \left(\mu / r\right)\right) \tag{5}$$

Substituting Eq. (5) into Eq. (4) and (3) results in the following required thrust direction and magnitude to maintain the displaced NKO:

$$\tan\alpha(\rho, h; \omega) = \frac{\rho}{h}\left(1 - \left(\omega/\omega_*\right)^2\right) \tag{6}$$

$$a(\rho, h; \omega) = \sqrt{\rho^2 \left(\omega^2 - \omega_*^2\right)^2 + h^2 \omega_*^4} \tag{7}$$

with ω_* the orbital angular velocity of a circular Keplerian orbit with a radius equal to the radius of the NKO:

$$\omega_* = \sqrt{\mu / r^3} = \sqrt{\mu / \left(\rho^2 + h^2\right)^{3/2}} \tag{8}$$

A. Out-of-plane displaced GEO

While the expressions derived above hold for any two-body displaced NKO, it is given for the displaced GEO that $\omega = \omega_{GEO} = \sqrt{\mu / r_{GEO}^3}$, with $r_{GEO} =$ 42164.1696 km. Furthermore, assuming a displacement h to create an out-of-plane displaced GEO, Eq. (7) can be used to find the corresponding projected radius ρ that minimizes the required acceleration. Taking the first derivative of Eq. (7) with respect to ρ and setting it equal to zero yields the following condition:

$$r^6 + \frac{\mu}{\omega^2} r^3 - 3\frac{\mu}{\omega^2} h^2 r - 2\left(\frac{\mu}{\omega^2}\right)^2 = 0 \tag{9}$$

The complex and negative real roots of this sixth order polynomial are ignored and Descartes' Rule of Signs is applied to find that Eq. (9) has one sign change and therefore one positive real root [23]. An analytical solution to Eq. (9) was not found, therefore a numerical method in the form of Newton's method was applied [24]. The results for a large range of out-of-plane displacements are illustrated in Fig. 2, which shows the acceleration contour plots for ω_{GEO} and includes the solution to Eq. (9). The figure shows the correctness of the approach as the solution connects the extrema of the separate contour lines, i.e. the minimum acceleration required to provide a particular out-of-plane displacement.

The figure furthermore shows that, clearly, the smaller the out-of-plane displacement, the smaller the required acceleration. However, for the displaced GEO, the minimum displacement is predefined by the geostationary station keeping box to prevent the spacecraft from interfering with other satellites in the GEO. Combining International Telecommunication Union (ITU) regulations and regulations drawn up by individual countries such as by the US Federal Communications Commission (FCC), a geostationary station keeping box of 0.1° - 0.2° can be defined, equaling a box size of 73.6 - 147.2 km centered around the geostationary satellite [25-26]. This leads to a range of displacement distances of 36.8 – 147.2 km, where 36.8 km represents the case that the spacecraft just hovers above

the GEO station keeping box, while the higher displacements also take a station keeping box for the displaced spacecraft into account. Three displacement distances will therefore be considered in this paper, namely 35, 75 and 150 km. Solving Eq. (9) for these three displacements and subsequently using Eq. (6) to find the required thrust acceleration pitch angle, provides the optimal displaced GEOs as defined in Table 1. From the pitch angle it becomes clear that an almost pure out-of-plane acceleration (i.e. $\alpha = 0$) is required. Eq. (6) subsequently shows that, to obtain $\alpha = 0$, the condition $\omega = \omega_*$ should be satisfied, which in its turn requires $r = r_{GEO}$. Substituting this into Eq. (6) and (7), gives the required thrust direction and magnitude to maintain such a displaced GEO:

$$\tan\alpha = 0 \tag{10}$$

$$a = h\omega_*^2 = \frac{\mu h}{r_{GEO}^3} \tag{11}$$

This type of orbit corresponds to a so-called 'Type I' NKO, which is stable for modest displacements [2]. A schematic of this type of out-of-plane displaced GEO is provided in Fig. 3. Contrary to the cases in Table 1, the Type I displaced GEO allows for an analytical derivation of the performance of hybrid sail control, and will therefore be used in this paper for the out-of-plane case. Especially since the difference in acceleration with respect to the minimized accelerations given in Table 1 is only 6.3×10^{-4} percent at maximum (i.e. for $h = 150$ km) and will therefore only result in a slightly conservative estimate of the performance.

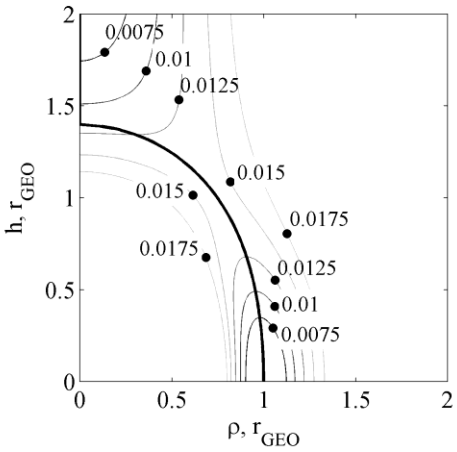

Fig. 2 Acceleration contour plots for ω_{GEO} including the minimized acceleration for a given out-of-plane displacement h. The acceleration is dimensionless with respect to the gravitational acceleration at unit planet radius and is marked on the contours.

Table 1 Definition of minimum acceleration out-of-plane displaced GEOs.

h , km	ρ , km	α , deg	a , mm/s^2
±35	42164.165	0.0476	0.1861
±75	42164.147	0.1019	0.3988
±150	42164.080	0.2038	0.7976

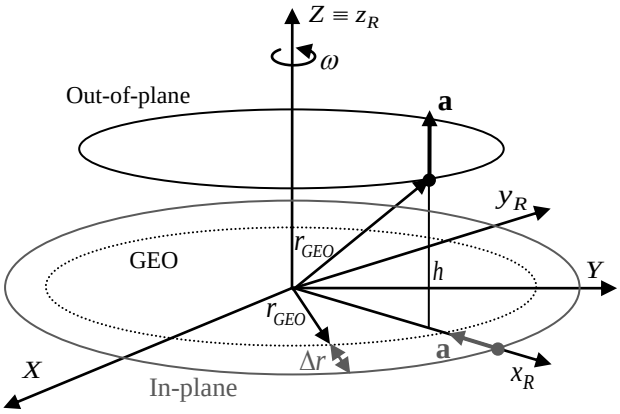

Fig. 3 Definition of out-of-plane and in-plane displaced GEOs.

B. In-plane displaced GEO

Rather than displacing the GEO out-of-plane, another option would be to displace the GEO in-plane, i.e. in the equatorial plane, see Fig. 3. Substituting $h = 0$ into Eq. (6) and (7) provides the thrust direction and magnitude required to maintain such an in-plane displaced GEO:

$$\alpha = \pm\frac{1}{2}\pi \tag{12}$$

$$a = \left|\rho\left(\omega_{GEO}^2 - \omega_*^2\right)\right| \tag{13}$$

with $\omega_* = \sqrt{\mu/\rho^3}$ and $\rho = r_{GEO} + \Delta r$, where the radial displacement $\Delta r > 0$ and $\Delta r < 0$ for orbits displaced outside or inside the GEO, respectively. Eq. (12) furthermore shows that a pure radial thrust is required, directed either inward ($\alpha < 0$) or outward ($\alpha > 0$), depending on the sign of Δr, to increase or decrease the angular velocity of a Keplerian orbit with radius ρ to the angular velocity of the GEO.

An initial assessment of the relative performance of the out-of-plane and in-plane displaced orbits can be derived from the contour plot in Fig. 2. The figure shows that for *small* and *equal* displacements in out-of-plane (along the vertical axis) and in-plane (along the horizontal axis) direction, the ratio of the required accelerations is

approximately 3, as can also be shown from Hill's equations [24]. The in-plane displacement thus requires an acceleration three times higher than an equally displaced out-of-plane orbit. The acceleration contours furthermore show that it is slightly more advantageous to displace the orbit outside ($\Delta r > 0$) the GEO than inside: for the same acceleration a larger displacement outside than inside the GEO can be achieved. This paper will therefore always consider the $\Delta r > 0$ case (as depicted in Fig. 3) for the in-plane displaced GEO.

II. Impulsive control

Although a continuous acceleration is required to achieve a displaced NKO, impulsive control using a chemical propulsion system can be employed to maintain a minimum displacement from a Keplerian orbit. By providing multiple impulsive velocity changes along the displaced GEO, the spacecraft can 'bounce' on the displaced orbit. Then, at time $t = 0$ the spacecraft is located at the displaced GEO and an instantaneous change in velocity, or impulse, ΔV , is given. This will cause the spacecraft to slightly move away from the displaced GEO. However, since no thrust is applied in between pulses, the spacecraft follows a natural Keplerian orbit after the impulse, causing the spacecraft to cross the displaced GEO after some time. Upon this crossing, another impulse is given to reverse the spacecraft velocity and start the cycle again. This concept is illustrated in Fig. 4 for an out-of-plane displaced GEO. The use of impulsive control to maintain displaced NKOs has been investigated before and has among others been suggested to hover above Saturn's rings [3, 27] and to maintain a local cluster of spacecraft for high resolution imaging of terrestrial or astronomical targets using interferometry techniques [28].

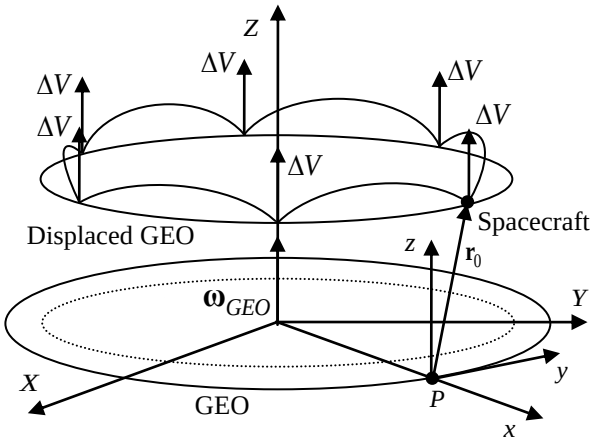

Fig. 4 Illustration of impulsive control for an out-of-plane displaced GEO and definition of reference frame for Hill's equations.

For small displacements, the required magnitude of the impulses can be computed using the linearized Hill's equations that represent the dynamics of a spacecraft in the vicinity of a point P on a circular Keplerian reference orbit, see Fig. 4 [3, 24]. A detailed derivation is given in Ref. [3] and is therefore not repeated here. Only the results are provided. For the first impulse the following holds:

$$\Delta V_{x,0} = \dot{x}_0 = \frac{3\omega_{GEO}^2 x_0 t_p \tan\left(\omega_{GEO} t_p/2\right)}{3\omega_{GEO} t_p - 8\tan\left(\omega_{GEO} t_p/2\right)} \tag{14}$$

$$\Delta V_{y,0} = \dot{y}_0 = 6x_0\omega_{GEO} \frac{\omega_{GEO} t_p - 2\tan\left(\omega_{GEO} t_p/2\right)}{8\tan\left(\omega_{GEO} t_p/2\right) - 3\omega_{GEO} t_p} \tag{15}$$

$$\Delta V_{z,0} = \dot{z}_0 = \omega_{GEO} z_0 \tan\left(\omega_{GEO} t_p/2\right) \tag{16}$$

with x_0 and z_0 defined in the rotating reference frame shown in Fig. 4 and $t_p = \tau/N$, where τ is the orbital period and N the number of impulses per orbit. For the out-of-plane displaced GEO $\dot{x}(t_p) = -\dot{x}(0)$, $\dot{y}(t_p) = \dot{y}(0)$ and $\dot{z}(t_p) = -\dot{z}(0)$ and therefore only repeated impulses in x and z direction have to be provided, but with double the required ΔV to reverse the direction of the velocity vector. For an in-plane displaced GEO $\dot{x}(t_p) = -\dot{x}(0)$, $\dot{y}(t_p) = \dot{y}(0)$ and $\dot{z}(t_p) = \dot{z}(0) = 0$, which requires only repeated, double magnitude impulses in x direction.

Fig. 5a shows the results for an out-of-plane displaced GEO levitated 35 km above the equatorial plane for one orbital revolution and for different numbers of impulses along the orbit. The top plot in Fig. 5b furthermore shows the ΔV required to maintain such an orbit, while the bottom plot provides similar information for a 35 km in-plane displaced orbit. The figure clearly shows the larger ΔV required for the in-plane case than for the out-of-plane case, as expected from the analysis in Section I.B. It also shows that a higher number of pulses is advantageous when displacing the orbit out-of-plane, i.e. the penalty on the ΔV due to pulsed rather than continuous control becomes less. Contrary, for the in-plane displaced GEO, a higher number of impulses is disadvantageous, because, although the amount of ΔV *per impulse* decreases, the decrease is not sufficient to compensate for the larger *number of impulses* that needs to be provided.

The analysis in Fig. 5 can be extended from one orbital revolution to multiple revolutions to obtain the performance of impulsive control for maintaining the displaced GEO in terms of mission lifetime. This lifetime, L, is defined as the epoch at which a particular mass fraction, m_f / m_0, is obtained:

$$m_f / m_0 = (m_0 - m_{prop}) / m_0 \tag{17}$$

with m_f, m_0 and m_{prop} the final, initial and propellant mass, respectively. The propellant mass can be computed through an iterative approach and using the rocket equation that gives the ratio of the mass prior (m^-) and after (m^+) the impulses providing the combined ΔV:

$$\frac{m^-}{m^+} = e^{\frac{\Delta V}{I_{sp} g_0}} \tag{18}$$

with I_{sp} the specific impulse and g_0 the Earth gravity constant. Eq. (18) in combination with the results in Fig. 5b immediately shows that the out-of-plane displaced GEO will outperform the in-plane displaced GEO due to the smaller amount of ΔV required. The results, as shown in Fig. 6, are therefore only provided for the out-of-plane case. Fig. 6 considers both a range of specific impulses (from current to near term and far-future technology) and a range of mass fractions for the three displacement distances of 35, 75 and 150 km. Furthermore, 10 impulses per orbit are assumed to provide a balance between the complexity of the mission, the penalty on the ΔV for pulsed control and the deviation from the nominal displaced orbit. Note that the symmetry of the problem causes the results for GEOs displaced above and below the equatorial plane to be exactly the same.

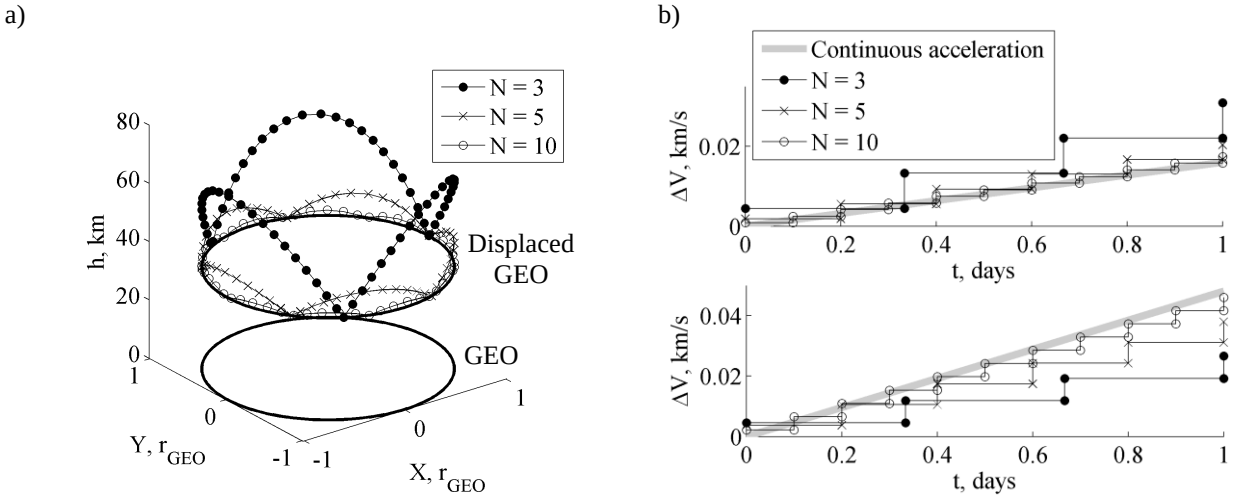

Fig. 5 (a) 35 km out-of-plane displaced GEO with impulsive control (b) Required ΔV for a 35 km out-of-plane (top) and in-plane (bottom) displaced GEO for different numbers of impulses per orbit N.

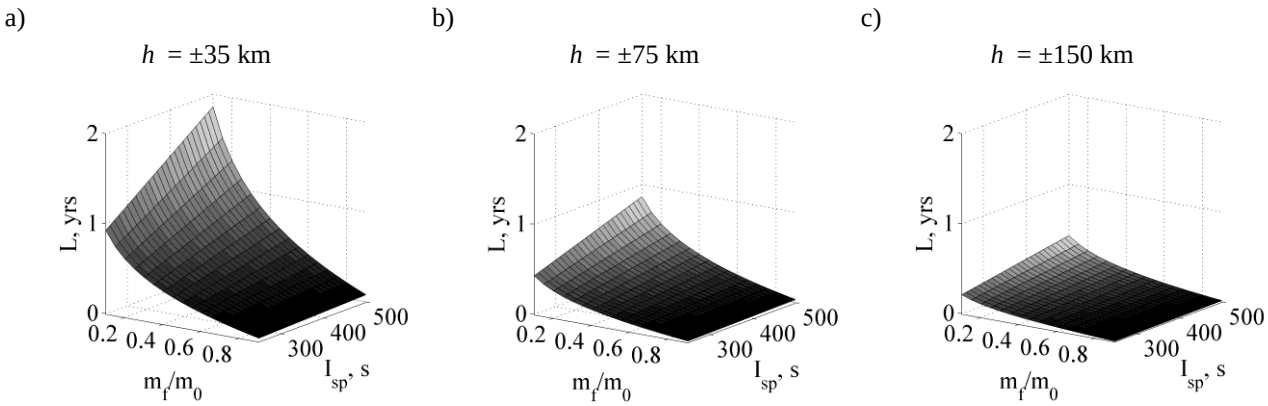

Fig. 6 Out-of-plane displaced GEOs maintained with impulsive control ($N=10$): mission time L as a function of the specific impulse I_{sp} and the mass fraction m_f / m_0 , for different values of the displacement distance h .

The graphs in Fig. 6 can be interpreted in different ways. For example, for a 35 km displaced GEO, an average specific impulse of 320 s [29] and a mass fraction of 0.5 a lifetime of 0.36 years can be achieved. Considering a lifetime of 10 - 15 years for current geostationary spacecraft, Fig. 6 shows that similar lifetimes cannot be achieved using impulsive control. Only a maximum of 1.9 years can be obtained for the smallest displacement distance and for extreme values of the specific impulse and the mass fraction. The cause of this poor performance lies in the penalty on the ΔV for pulsed rather than continuous control and the low specific impulse of chemical propulsion systems.

III. SEP control

This section investigates the use of SEP to maintain the displaced GEO in order to improve the performance of the displaced GEO with respect to the use of impulsive control. The performance of SEP control in terms of mission lifetime for a particular mass fraction can be assessed by considering the following differential equation for the mass:

$$\dot{m} = -\frac{T}{I_{sp} g_0} \tag{19}$$

with T the SEP thrust magnitude. Since the required acceleration is constant (see Eq. (7)), the lifetime can be derived analytically from Eq. (19). Substituting $T = a \cdot m$ into Eq. (19) and rearranging gives:

$$\int_{m_0}^{m_f} \frac{dm}{m} = -\int_{t_0}^{t_f} \frac{a}{I_{sp} g_0} dt \tag{20}$$

Evaluating these integrals and setting $t_0 = 0$ yields the following lifetime:

$$L = t_f = \ln\left(\frac{m_0}{m_f}\right)\frac{I_{sp} g_0}{a} \tag{21}$$

Eq. (21) shows that, clearly, a higher required acceleration reduces the mission lifetime. Considering the fact that the in-plane displaced GEO requires a larger acceleration than an equally displaced orbit out-of-plane (see Section I.B), a shorter lifetime can be expected for the in-plane case. The results, as shown in Fig. 7, are therefore again only provided for the out-of-plane case.

Fig. 7 shows the mission lifetime for an arbitrary initial mass, a wide range of specific impulses and mass fractions and for the three displacement distances of 35, 75 and 150 km. Again, the results hold both for GEOs displaced above the equatorial plane and for those displaced below the equatorial plane, due to the symmetry of the problem.

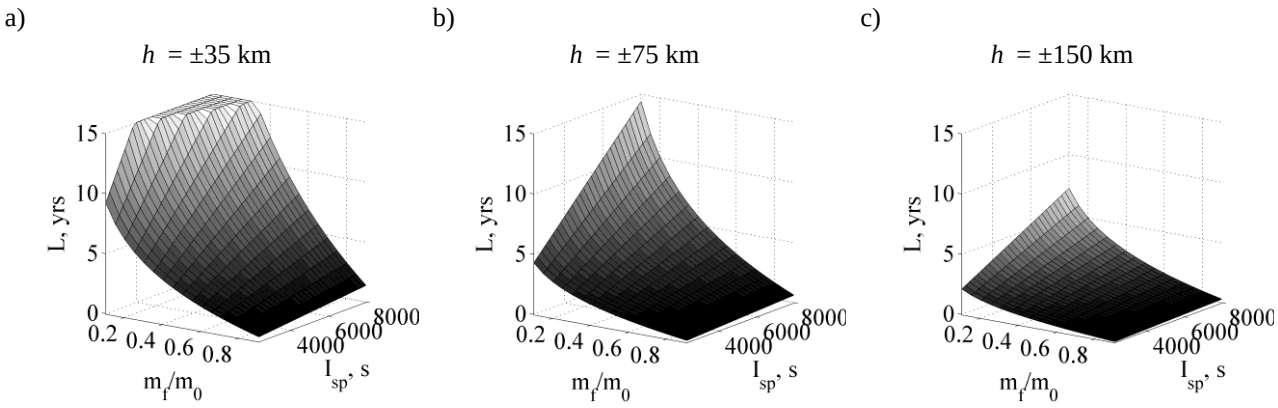

Fig. 7 Out-of-plane displaced GEOs maintained with SEP control: mission time L (a maximum of 15 years is considered) as a function of the specific impulse I_{sp} and the mass fraction m_f / m_0, for different values of the displacement distance h.

The graphs can be interpreted similarly to the graphs in Fig. 6. Comparing Fig. 7 with Fig. 6 immediately shows a dramatic improvement of the lifetime for an SEP controlled spacecraft over an impulsive controlled spacecraft. Again, considering a mass fraction of 0.5 and assuming a currently feasible SEP specific impulse of 3200 s (e.g. as flown on the Hayabusa spacecraft [30]), the lifetime is increased from 4.3, 2.0 and 1.0 months for impulsive control to 3.7, 1.7 and 0.9 years for 35, 75 and 150 km displaced orbits, respectively. However, lifetimes of 10 - 15 years as

for current geostationary spacecraft can still only be achieved for the smallest displacement of 35 km and either for low mass fractions (e.g. $m_f = 0.1$ and $I_{sp} = 2600$ s) or for high specific impulses (e.g. $m_f = 0.45$ and $I_{sp} = 7500$ s).

IV. Hybrid sail control

To improve the performance of the displaced GEO even further, this section will investigate the use of hybrid sail control. For this, the acceleration required to maintain the displaced GEO, $\mathbf{a}$, see Eq. (1) or equivalently Eq. (10) and (11) for the out-of-plane case and Eq. (12) and (13) for the in-plane case, is written as the sum of the acceleration generated by the SEP system, $\mathbf{a}_{SEP}$, and the acceleration produced by the solar sail, $\mathbf{a}_s$:

$$\mathbf{a} = \mathbf{a}_{SEP} + \mathbf{a}_s \tag{22}$$

To maximize the lifetime of the mission, the objective is to minimize the magnitude of the acceleration required from the SEP system:

$$\min\left(a_{SEP}\right) = \min\left(\left\|\mathbf{a} - \mathbf{a}_s\right\|\right) \tag{23}$$

where the acceleration generated by the solar sail is given by:

$$\mathbf{a}_s = \beta \frac{\mu_S}{r_s^2}\left(\hat{\mathbf{n}} \cdot \hat{\mathbf{r}}_s\right)^2 \hat{\mathbf{n}} \tag{24}$$

with μ_S the gravitational parameter of the Sun. Note that an ideal, i.e. a perfectly reflecting, sail is assumed. The unit vector in the direction of the solar radiation pressure force, $\hat{\mathbf{n}}$, is therefore directed normal to the sail surface. Furthermore, the magnitude of the Sun-sail vector, $\left\|\mathbf{r}_s\right\|$, is approximated by a constant Sun-Earth distance of 1 AU. The parameter β is the solar sail lightness number and can be defined as the ratio of the solar radiation pressure acceleration and the solar gravitational acceleration, or equivalently as the ratio of the system loading (i.e. the ratio of the spacecraft mass to the solar sail area, $\sigma = m / A_s$) and the critical sail loading, $\sigma^* = 1.53$ g/m^2 [2]:

$$\beta = \frac{\sigma^*}{\sigma} \tag{25}$$

Eq. (25) shows that for a sail loading equal to the critical sail loading, the lightness number is unity, indicating that the solar radiation pressure acceleration is exactly equal to the solar gravitational acceleration. The equation furthermore shows that the sail lightness number is a function of the spacecraft mass. Since the mass of the hybrid

sail spacecraft decreases due to the consumption of propellant by the SEP system, the parameter β increases according to:

$$\beta = \beta_0 \frac{m_0}{m} \tag{26}$$

where the subscript '0' indicates the start of the mission.

Due to the tilt of the Earth's rotational axis with respect to the ecliptic plane, the direction of the Sun-sail unit vector $\hat{\mathbf{r}}_s$ changes during the year. To model this variation, an Earth fixed rotating reference frame $E(x_E, y_E, z_E)$ as shown in Fig. 8 is used. Centered at the Earth with the (x_E, y_E) plane in the equatorial plane and the z_E axis along the rotational axis of the Earth, this reference frame rotates with the same angular velocity as the Earth in its orbit around the Sun, causing the unit vector $\hat{\mathbf{r}}_s$ to always be contained in the (x_E, z_E) plane. The angle χ describes the position of the Earth along its orbit (with χ =0 at winter solstice), while the angle ψ is defined as the angle between $\hat{\mathbf{r}}_s$ and the equatorial plane and is therefore a function of χ. This angle is at its maximum at winter solstice ($\psi(0) = i_{obl}$) and at its minimum at summer solstice ($\psi(\pi) = -i_{obl}$) with i_{obl} the obliquity of the ecliptic.

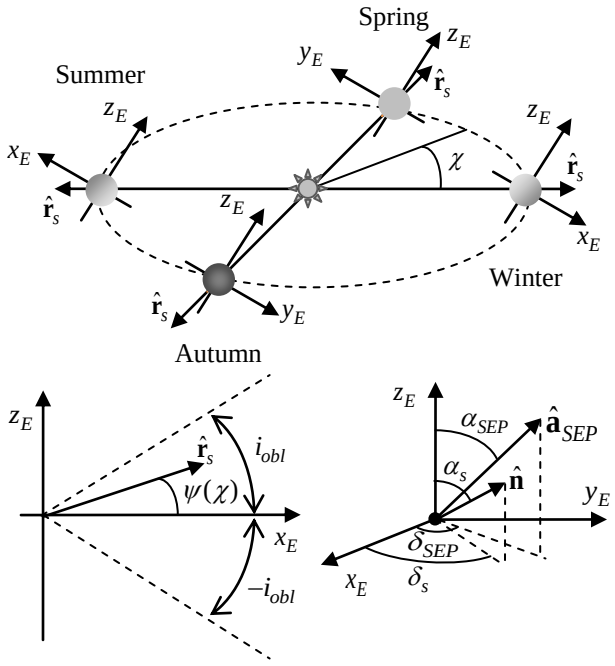

Fig. 8 Definition of reference frame and parameters used to model the seasonal variation of $\hat{\mathbf{r}}_s$ and to define the solar sail and SEP pitch and yaw angles.

The variation of ψ is in magnitude equal to the solar declination, but is opposite in sign:

$$\psi(\chi) = \sin^{-1}\left(\sin i_{obl} \cos \chi\right) \tag{27}$$

yielding:

$$\hat{\mathbf{r}}_s = \begin{pmatrix} \cos\psi \\ 0 \\ \sin\psi \end{pmatrix} \tag{28}$$

The unit vector normal to the sail surface, $\hat{\mathbf{n}}$, can be described using the same frame of reference, see Fig. 8. Using the solar sail pitch angle, α_s, and yaw angle, δ_s, the unit vector $\hat{\mathbf{n}}$ is given by:

$$\hat{\mathbf{n}} = \begin{pmatrix} \sin\alpha_s \cos\delta_s \\ \sin\alpha_s \sin\delta_s \\ \cos\alpha_s \end{pmatrix} \tag{29}$$

Substituting Eq. (29) and the expressions for $\hat{\mathbf{r}}_s$, $\hat{\mathbf{n}}$ and β into Eq. (22) and rearranging gives:

$$\begin{aligned} a_{SEP,x_E} &= a_{x_E} - \beta_0 \frac{m_0}{m} \frac{\mu_S}{r_s^2} (\cos\psi \sin\alpha_s \cos\delta_s \\ &\quad + \sin\psi \cos\alpha_s)^2 \sin\alpha_s \cos\delta_s \\ a_{SEP,y_E} &= a_{y_E} - \beta_0 \frac{m_0}{m} \frac{\mu_S}{r_s^2} (\cos\psi \sin\alpha_s \cos\delta_s \\ &\quad + \sin\psi \cos\alpha_s)^2 \sin\alpha_s \sin\delta_s \\ a_{SEP,z_E} &= a_{z_E} - \beta_0 \frac{m_0}{m} \frac{\mu_S}{r_s^2} (\cos\psi \sin\alpha_s \cos\delta_s \\ &\quad + \sin\psi \cos\alpha_s)^2 \cos\alpha_s \end{aligned} \tag{30}$$

with a_{x_E}, a_{y_E} and a_{z_E} the components of the acceleration required to maintain the displaced GEO as defined in Eq. (10) and (11) for the out-of-plane case and in Eq. (12) and (13) for the in-plane case. For instance, for the out-of-plane case, $a_{x_E} = a_{y_E} = 0$ and $a_{z_E} = \mu h / r_{GEO}^3$. In that case, the SEP system thus needs to counterbalance the in-plane component of the solar sail acceleration and needs to augment the out-of-plane solar sail acceleration to obtain the required out-of-plane acceleration.

Inspecting Eq. (30) shows that for a given value for m and ψ (i.e. for a particular instant of time), the minimization problem in Eq. (23) is merely a function of the solar sail pitch and yaw angles and therefore reduces to finding the optimal solar sail pitch and yaw angles that minimize the acceleration required from the SEP system:

$$\left(\alpha_s^*, \delta_s^*\right) = \underset{\substack{\alpha_s \in \left[\alpha_{s,\min}, \alpha_{s,\max}\right] \\ \delta_s \in [-\pi, \pi]}}{\arg\min} \left(a_{SEP}(\alpha_s, \delta_s)\right) \tag{31}$$

where the domain of α_s is defined later in the paper. The next two subsections solve this minimization problem for the out-of-plane and in-plane cases separately.

A. Out-of-plane displaced GEO

For the out-of-plane case, the solution to Eq. (31) can be found by setting the partial derivative of the SEP acceleration with respect to the sail pitch and yaw angles equal to zero:

$$\frac{\partial a_{SEP}}{\partial \alpha_s} = \frac{\partial a_{SEP}}{\partial \delta_s} = 0 \tag{32}$$

Performing this analysis for the yaw angle yields:

$$\begin{gathered} \frac{\partial a_{SEP}}{\partial \delta_s} = -4c_1\left(\hat{\mathbf{n}}\cdot\hat{\mathbf{r}}_s\right)\left(c_1\left(\hat{\mathbf{n}}\cdot\hat{\mathbf{r}}_s\right)^2 - c_2\cos\alpha_s\right) \\ \cos\psi\sin\alpha_s\sin\delta_s = 0 \end{gathered} \tag{33}$$

with

$$c_1 = \beta_0 \frac{m_0}{m}\frac{\mu_S}{r_s^2}, \quad c_2 = \frac{\mu h}{r_{GEO}^3} \tag{34}$$

For Eq. (33) to hold throughout the year and considering that $c_1 \neq 0$ and $(\hat{\mathbf{n}}\cdot\hat{\mathbf{r}}_s) > 0$ (to generate a solar sail acceleration) the optimal yaw angle equals:

$$\delta_s^* = n\pi \tag{35}$$

with n an integer equaling either 0 or 1. Substituting this value into Eq. (30) (with $a_{x_E} = a_{y_E} = 0$ and $a_{z_E} = \mu h / r_{GEO}^3$) shows that the y_E component of the SEP thrust force is zero at all times. Furthermore, considering the fact that the solar sail is unable to generate a thrust component in the direction of the Sun and recalling that the x_E axis points away from the Sun at all times, Eq. (35) can be reduced to:

$$\delta_s^* = 0 \tag{36}$$

A similar analysis can be performed for the partial derivative with respect to the sail pitch angle. Substituting $\delta_s = \delta_s^* = 0$ gives the following condition:

$$\sin(\alpha_s+\psi)-\frac{c_2}{c_1}\frac{\cos\alpha_s}{\sin(\alpha_s+\psi)}+\frac{c_2}{2c_1}\frac{\sin\alpha_s}{\cos(\alpha_s+\psi)}=0 \tag{37}$$

An analytical solution for the optimal pitch angle was not found from this expression, therefore Newton's method is once more applied to find α_s^*. To ensure that the optimal pitch angle does not generate a normal vector $\hat{\mathbf{n}}$ pointing towards the Sun, bounds are imposed on the optimum pitch angle, as depicted in Fig. 9 for two epochs during the year. Furthermore, by requiring α_s to be contained in the first two and last two quadrants for orbits displaced above and below the equatorial plane, respectively, $\partial^2 a_{SEP}/\partial\alpha_s^{\,2}>0$ is ensured such that the solution corresponds to a minimum rather than a maximum of $a_{SEP}(\alpha_s,\delta_s)$.

Note that Fig. 9 clearly illustrates that the out-of-plane displaced GEO as presented in this paper cannot be maintained throughout the year using only a solar sail. For instance, in summer the shaded area shows that the required thrust direction for a displaced GEO displaced *above* the equatorial plane (i.e. a thrust along the positive z_E axis) cannot be achieved by the solar sail. A similar reasoning holds for a GEO displaced *below* the equatorial plane in winter. Furthermore, in autumn and spring the required thrust direction for orbits displaced both above and below the equator lies on the edge of the shaded half-circle. The magnitude of the solar sail acceleration along the z_E axis in that case becomes equal to zero as the Sun shines edge-on to the solar sail.

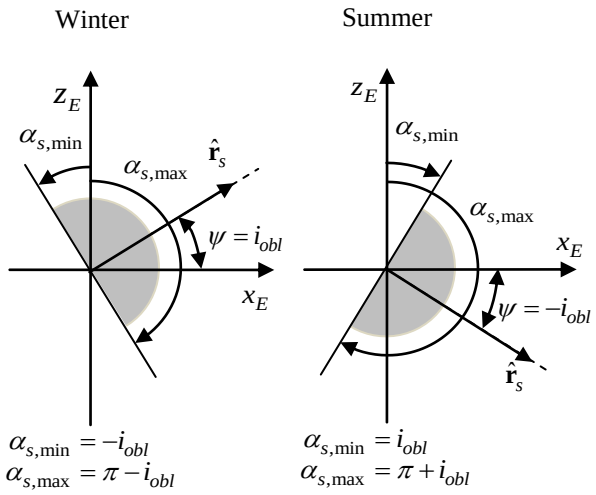

Fig. 9 Definition of minimum and maximum solar sail pitch angles during the year.

Once the optimal sail pitch and yaw angles are found, the magnitude and direction of the acceleration required from the SEP system can be computed. Using Eq. (30), the pitch and yaw angles of the SEP thrust force, α_{SEP} and δ_{SEP} respectively, can be computed, see Fig. 8:

$$\begin{aligned} \alpha_{SEP} &= \text{acos}\left(\frac{a_{SEP,z_E}}{a_{SEP}} \right) \\ \delta_{SEP} &= \text{atan2}\left(a_{SEP,y_E}, a_{SEP,x_E} \right) \end{aligned} \tag{38}$$

as well as the magnitude of the required SEP thrust force:

$$T = m \cdot a_{SEP} \tag{39}$$

Previously it was already stated that $a_{SEP,y_E} = 0$ since $\delta_s^* = 0$. Substituting $a_{SEP,y_E} = 0$ into Eq. (38) gives a constant SEP yaw angle of $\delta_{SEP} = n\pi$, again with n an integer equaling either 0 or 1.

As noted before, the above holds for one instant in time, i.e. for a given value for m and ψ. To find the variation of the controls, accelerations, thrust magnitude and mass as a function of time over multiple orbital periods, the displaced GEO is discretized into several nodes. The nodes are equally distributed over the orbit, leading to a constant time interval Δt in between two consecutive nodes. At each node, i, the required SEP thrust magnitude can be approximated using Eq. (39) as $T_i = m_i \cdot a_{SEP,i}$. Then, assuming a constant thrust magnitude during the interval Δt, the mass at the end of the i^{th} interval can be approximated through the recurrence relation:

$$m_{i+1} = m_i - \frac{T_i}{I_{sp} g_0} \Delta t \tag{40}$$

At each node the optimum solar sail angles (and subsequently the SEP acceleration, thrust angles and thrust magnitude) can be computed. When changing from one node to the successive node, the change in ψ can be computed using Eq. (27), while the mass at the start of the new interval can be computed using Eq. (40).

The results after one year in a GEO displaced 35 km along the positive z_E axis are shown in Fig. 10 and by the solid lines in Fig. 11. A time interval of $\Delta t = 0.005$ days is adopted, which is considered to be small enough to allow for a fair comparison later in the paper with the analytical analysis for SEP control in Section III. Furthermore, an initial mass of 1500 kg (the smaller class of geostationary spacecraft [31]) and a specific impulse of 3200 s are

assumed. Finally, four different values for the sail lightness number are considered, $\beta_0 = 0.01$, 0.05, 0.1 and 0.2, where a value of 0.05 can be assumed reasonable for near-term systems [32].

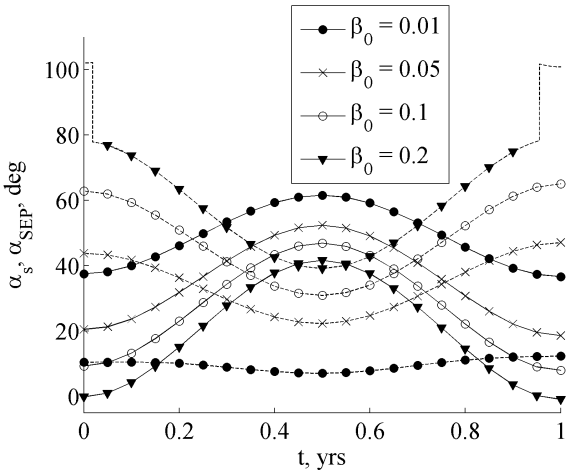

Fig. 10 Optimal solar sail (solid lines) and SEP (dashed lines) pitch angles for a 35 km out-of-plane displaced GEO maintained with hybrid sail control for different values of the solar sail lightness number β_0.

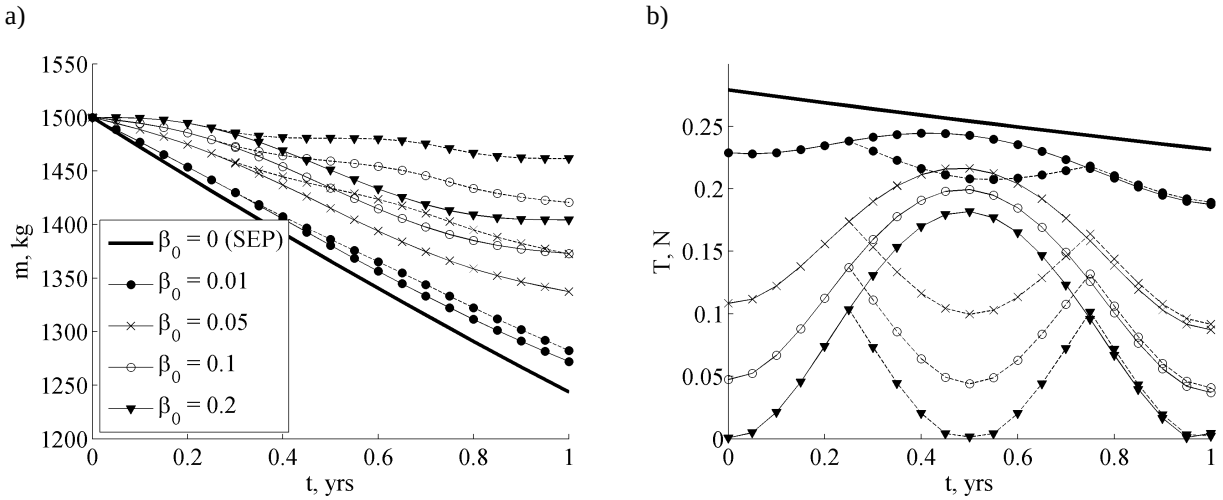

Fig. 11 35 km out-of-plane displaced GEO maintained with hybrid sail control for different values of the solar sail lightness number β_0. Spacecraft mass (a) and required SEP thrust magnitude (b) assuming an initial mass of 1500 kg and a specific impulse of 3200 s. Solid lines indicate a year-long displacement along the positive z_E axis. Dashed lines include a seasonal transfer between north and south displaced GEOs.

Fig. 10 shows that the optimal pitch angle of the solar sail decreases and the pitch angle of the SEP thruster increases for increasing values of β_0, indicating a larger contribution from the sail to the required out-of-plane acceleration for larger values of β_0. It also indicates a shift in the main task of the SEP thruster from providing the out-of-plane acceleration to compensating the in-plane component of the sail acceleration. Furthermore, some discontinuities can be observed in the profile of the SEP pitch angle for the largest value of β_0. This large value for β_0 causes the component of the solar sail acceleration along the positive z_E axis to become larger than the required out-of-plane acceleration. This requires the SEP thruster to thrust along the negative z_E axis to counterbalance the access out-of-plane acceleration, hence the switch in the SEP pitch angle from $\alpha_{SEP} < \pi/2$ to $\alpha_{SEP} > \pi/2$.

In general, the larger the value for β_0 the lower the demand on the SEP system, which is directly translated into a larger final mass after 1 year in orbit when using hybrid sail control instead of SEP control, see Fig. 11a. Already a solar sail with β_0 = 0.01 provides a gain in propellant mass of 29 kg. Further increasing β_0 results in savings of 94, 130 and 161 kg for β_0 = 0.05, 0.1 and 0.2, respectively.

Finally, considering the required thrust magnitude in Fig. 11b, another advantage of hybrid sails over pure SEP becomes evident. While the thrust level required for a 1500 kg spacecraft with SEP control is larger than currently achievable thrust levels of 0.2 N for this spacecraft size (e.g. EADS/Astrium RIT-XT), thrust levels smaller than 0.2 N throughout the year can be observed for β_0 = 0.1 and 0.2. Even for β_0 = 0.05 the thrust level remains well under 0.2 N during winter, but it is higher during summer. This performance can be improved by transferring the spacecraft from a GEO displaced above the equatorial plane (north) in winter to an orbit displaced below the equatorial plane (south) in summer. Then, the performance of the sail is no longer limited by the obliquity of the ecliptic and can perform equally well in summer as it does in winter above the equatorial plane.

When this so-called ‘seasonal transfer’ is introduced in the model, results as presented by the dashed lines in Fig. 11 are obtained. Note that the mission is assumed to always start in winter, i.e. above the equatorial plane, and that an instantaneous seasonal transfer is considered. As expected, massive improvements both in terms of propellant consumption and required thrust levels can be observed. The mass savings mentioned before are now increased to 39, 129, 178 and 219 kg for β_0 = 0.01, 0.05, 0.1 and 0.2, respectively. At the end of this paper, it will be shown that

transfers from above to below the equatorial plane and vice versa are possible and come at the cost of a negligible to modest SEP propellant consumption.

While the results in Fig. 10 and Fig. 11 only hold for a mission lifetime of one year, it is interesting to investigate whether hybrid propulsion can enable out-of-plane displaced GEO missions lasting as long as current geostationary missions. Previous sections already showed that impulsive and SEP control are unable to do so. Extending the mission lifetime for hybrid sail control results in the graphs of Fig. 12. Note that all results neglect the effects of eclipses on the performance of the solar sail. For the (displaced) GEO, eclipses occur for a short period per day around the equinoxes. It is assumed that increased SEP thrust can compensate for the absence of thrust from the solar sail during these brief periods.

Fig. 12 includes both cases of excluding and including the seasonal transfer and shows that the seasonal transfer can significantly increase the mission lifetime from a few months for the smaller values for β_0 up to a few years for the larger values for β_0. Furthermore, comparing Fig. 12 with Fig. 6 and Fig. 7 shows a dramatic improvement of the lifetime for hybrid sail control compared to both impulsive and SEP control. For small displacement distances even lifetimes of 10 - 15 years come into reach and the lifetime for the larger displacements become reasonable. Again, comparing the lifetimes for a mass fraction of 0.5 and a specific impulse of 3200 s increases the lifetime for a 35 km out-of-plane displaced orbit from 3.7 years for SEP control to 4.4 - 9.2 years (depending on the value chosen for β_0) when the seasonal transfer is not included and to 4.7 - 15 years when the transfer is included. Similarly, the lifetimes for a 150 km out-of-plane displaced orbit are increased from 0.9 years to 0.9 - 1.2 years (excluding transfer) and to 0.9 - 1.4 years (including transfer).

B. Comparison with in-plane displaced GEO

Although the analyses performed in Sections II and III showed that the out-of-plane displaced GEO outperforms the in-plane displaced GEO for the use of impulsive and SEP control, it is still worthwhile to investigate the performance of the in-plane displaced GEO for the use of hybrid sails. The reason for this is the fact that, despite the larger required acceleration to maintain the in-plane displaced GEO, the direction of this acceleration is much more favorable as it is approximately along the Sun-sail line in parts of the orbit.

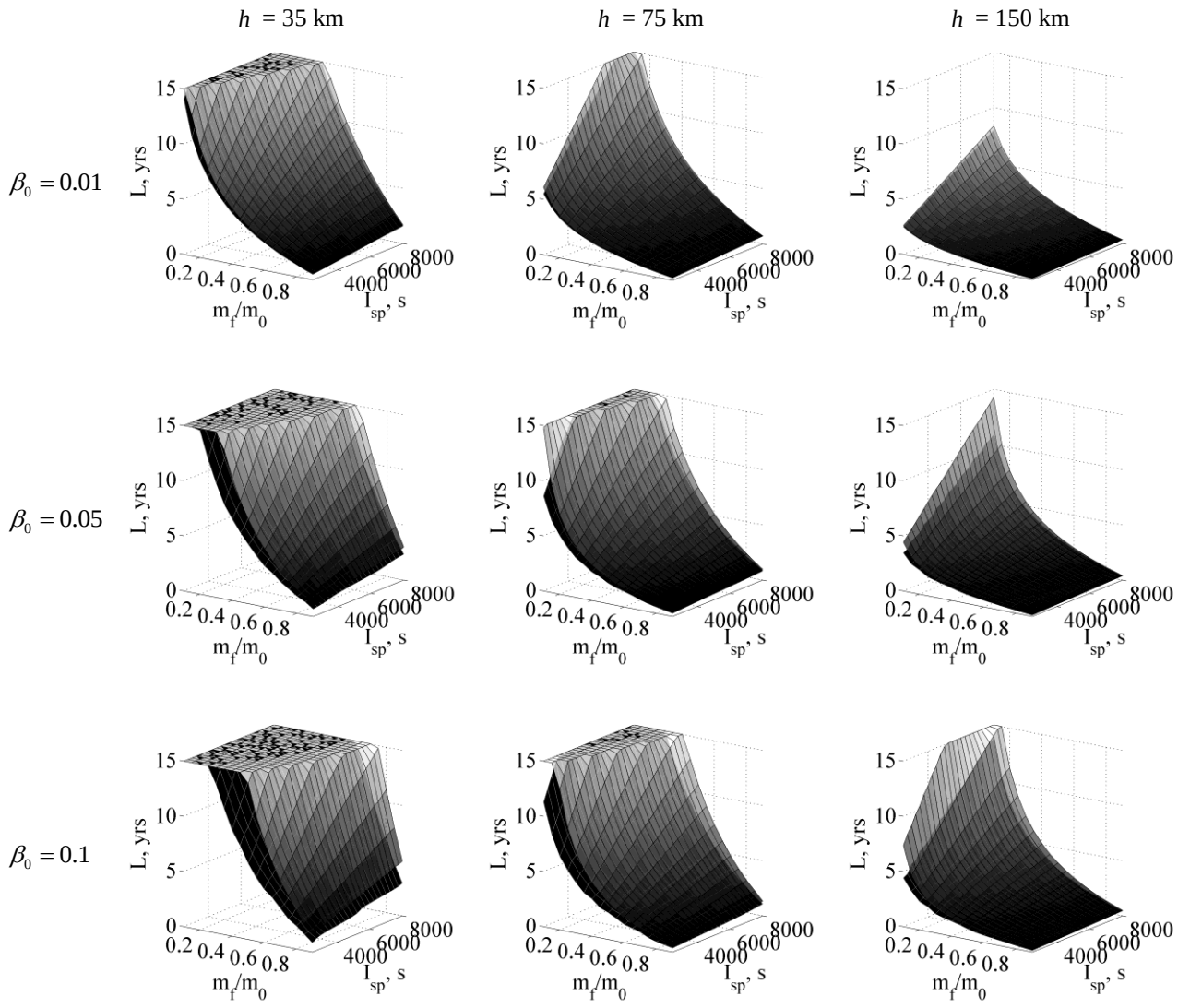

Fig. 12 Out-of-plane displaced GEOs maintained with hybrid sail control: mission time L (a maximum of 15 years is considered) as a function of the specific impulse I_{sp} and the mass fraction m_f / m_0, for different values of the displacement distance h and the sail lightness number β_0. The solid surfaces exclude a seasonal transfer between north and south displaced GEOs. The transparent surfaces include this transfer.

To investigate the performance of hybrid sails for the in-plane displaced GEO, the minimization problem in Eq. (31) needs to be solved with $a_{x_E} = \rho\left(\omega_{GEO}^2 - \omega_*^2\right)\cos\theta_E$, $a_{y_E} = \rho\left(\omega_{GEO}^2 - \omega_*^2\right)\sin\theta_E$ and $a_{z_E} = 0$, where θ_E is the angular position in the displaced GEO, measured from the positive x_E axis in counterclockwise direction. Applying the same approach as used in Section IV.A to solve for the optimum solar sail pitch and yaw angles would required a system of nonlinear equations to be solved using the Newton method rather than the single expression in Eq. (37).

Therefore, the minimization problem is solved using a sequential quadratic programming (SQP) method implemented in the MATLAB® function *fmincon* [33]. This function allows to define the bounds for the sail pitch angle α_s as shown in Fig. 9 and include a constraint to ensure $(\hat{\mathbf{n}} \cdot \hat{\mathbf{r}}_s) \geq 0$. As for the out-of-plane case, the displaced GEO is discretized into nodes, again with a time interval of $\Delta t = 0.005$ days, and at each node the minimization problem of Eq. (31) is solved. The results for a 35 km displaced orbit are provided in Fig. 13 and Fig. 14. Fig. 13 clearly illustrates the influence of the changing direction of the Sun-sail line during the year and the sail attitude constraint that prevents the sail from generating an acceleration in the direction of the Sun. The latter requires the sail to be turned 180° every orbit and almost instantaneously during the equinoxes. However, as expected, during parts of the in-plane displaced orbit (around $\theta_E = 0$) the sail normal is aligned with the required, radial acceleration, which significantly lowers the demand on the SEP thruster, see Fig. 14. This figure provides the acceleration required by the SEP thruster for both in-plane (solid lines) and out-of-plane (dashed lines) displaced GEOs for different values of the sail lightness number and during the solstices (Fig. 14a) and the equinoxes (Fig. 14b). The favourable Sun-sail line and required radial acceleration even causes the SEP acceleration for the in-plane case to be lower than for the out-of-plane case during the equinoxes and for $\beta_0 = 0.1$. However, during the remainder of the orbit, the sail attitude constraint restricts the sail to such extent that the SEP thruster has to provide the greater part of the required acceleration, causing the out-of-plane case to outperform the in-plane case also for the use of hybrid sails.

a) b)

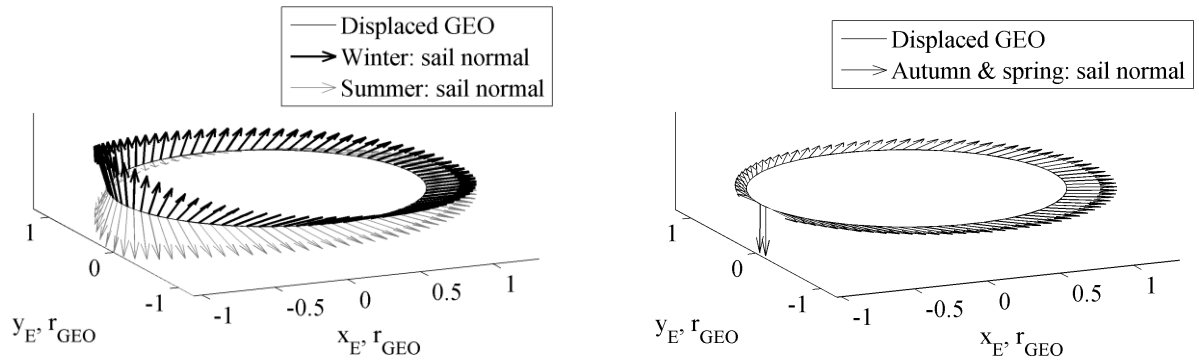

Fig. 13 Solar sail normal vector ($\beta_0 = 0.1$) for a 35 km in-plane displaced GEO during the solstices (a) and equinoxes (b).

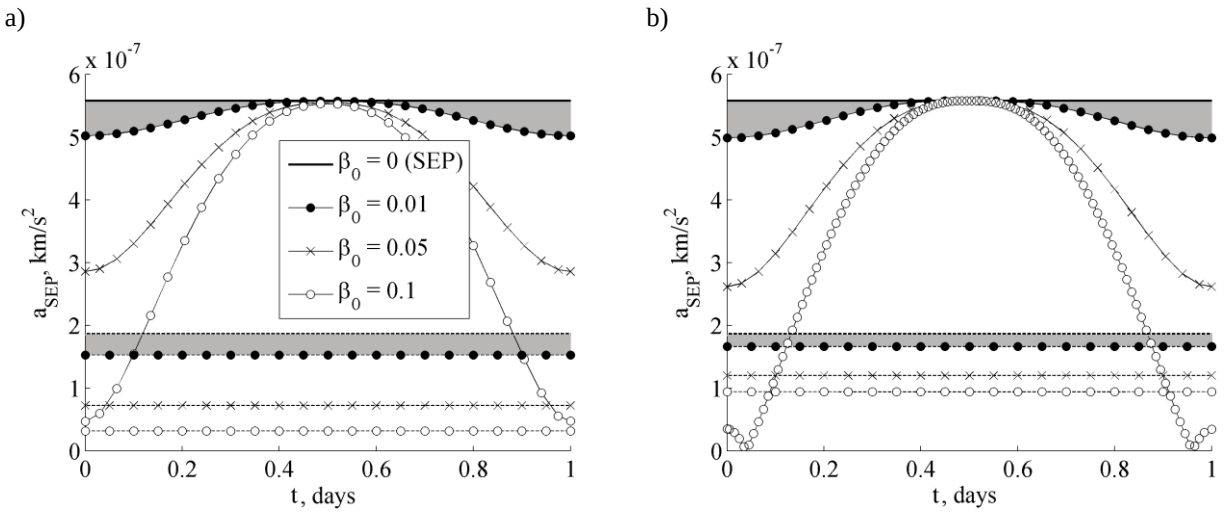

Fig. 14 Required SEP acceleration for a 35 km in-plane (solid lines) and out-of-plane (dashed lines) displaced GEO for different values of the sail lightness number β_0 and during the solstices (a) and the equinoxes (b). The shaded areas illustrate the contribution from the solar sail for $\beta_0 = 0.01$.

Since all types of propulsion considered show a much better performance for the out-of-plane displaced GEO than for the in-plane displaced GEO, the remainder of this paper, i.e. the mass budget analysis and the transfer trajectories will focus solely on the out-of-plane displaced GEO.

V. Mass budget

The results in Fig. 6, Fig. 7 and Fig. 12 provide the performance of impulsive, SEP and hybrid sail control for an out-of-plane displaced GEO in terms of propellant consumption. However, the goal of the mission is to maximize the lifetime of a spacecraft carrying a given payload. It should therefore be investigated whether the mass fractions and specific impulses of Fig. 6, Fig. 7 and Fig. 12 allow for any payload mass to be left at the lifetimes shown in those figures. For this, the spacecraft mass budget is investigated. However, due to its poor performance, impulsive control is discarded as a viable option to maintain the out-of-plane displaced GEO and this section will therefore only consider the mass budget for a hybrid sail and SEP propelled spacecraft. The corresponding mass budgets are based on what is proposed in Ref. [34]:

$$m_0 = m_{prop} + m_{tank} + m_{SEP} + m_P + m_{gimbal} + m_s + m_{pay} \tag{41}$$

The initial mass is broken down into seven elements. First, a propellant mass, m_{prop}, that follows from the initial and final spacecraft mass (see Eq. (19) and Eq. (40)), where the final mass is obtained after a certain lifetime L. Then, the mass of the tanks required to store the propellant, $m_{tank} = 0.1 m_{prop}$ [35], and the mass of the SEP thruster, which is a function of the maximum power required by the SEP subsystem, $P_{SEP,\max}$, which on its own is a function of the maximum thrust required during the mission, $T_{\max}$:

$$\begin{aligned} m_{SEP} &= k_{SEP} P_{SEP,\max} \\ P_{SEP,\max} &= \frac{T_{\max} I_{sp} g_0}{2\eta_{SEP}} \end{aligned} \tag{42}$$

with $k_{SEP} = 0.02$ kg/W [29] the specific performance of the SEP thruster and $\eta_{SEP} = 0.7$ [36] its efficiency. Subsequently, in the case of SEP control a solar array with mass $m_P = k_{SA} P_{SEP,\max}$ is assumed to provide electrical energy to the SEP system with $k_{SA} = 1/45$ kg/W the specific performance of the solar array [29]. In case of hybrid sail control, it is assumed that part of the sail is covered with thin film solar cells for this purpose. The required area covered with solar cells can be computed from the maximum power required by the SEP system:

$$A_{TF} = \frac{P_{SEP,\max}}{W \eta_{TF}} \cos \gamma_{SEP,\max} \tag{43}$$

The efficiency of the thin film is set to a conservative value of $\eta_{TF} = 0.05$ and $\gamma_{SEP,\max}$ represents the angle between the Sun-sail line and the solar sail normal vector when $T = T_{\max}$. From Eq. (43) the mass of the thin film $m_P = \sigma_{TF} A_{TF}$ can be computed with $\sigma_{TF} = 100$ g/m^2 [37]. Note that the influence of the thin film solar cells on the performance of the sail is neglected in this paper. Then, the mass of a gimbal, $m_{gimbal} = 0.3 m_{SEP}$ [35], is taken into account to ensure that the solar sail and SEP thruster can steer independently of one another. Finally, the mass of the sail can be computed through $m_s = \sigma_s A_s$ with σ_s the mass per unit area of the solar sail and the area of the sail, A_s, given through:

$$A_s = \frac{\beta_0 m_0}{\sigma^*} + A_{TF} \tag{44}$$

For the sail loading σ_s a value of 5 g/m^2 is assumed, which is optimistic, but considered reasonable for future solar sail missions as shown in recent studies [38-39]. Clearly, for an SEP controlled spacecraft, both m_{gimbal} and m_s are set to zero.

For a given mission lifetime and for a particular specific impulse, the only unknowns for computing the payload mass are the initial mass and the maximum SEP thrust required during the mission, $T_{\max}$, which are related since the initial mass is bounded by $T_{\max}$. For SEP control, this maximum thrust occurs at $t = t_0$ causing $T_{\max} = T_0$. With the required acceleration to maintain the out-of-plane displaced GEO given for a particular displacement distance, the maximum initial mass can be computed through $m_{0,\max} = T_0 / a$. However, for hybrid sail control, the maximum thrust does not necessarily occur at $t = t_0$, but can also occur in autumn (when the seasonal transfer is taken into account, as is done in this section) as shown in Fig. 11b. The resulting maximum initial masses for both SEP and hybrid sail control are provided in Fig. 15 as a function of the maximum thrust magnitude and for each of the displacement distances used so far and for different sail lightness numbers.

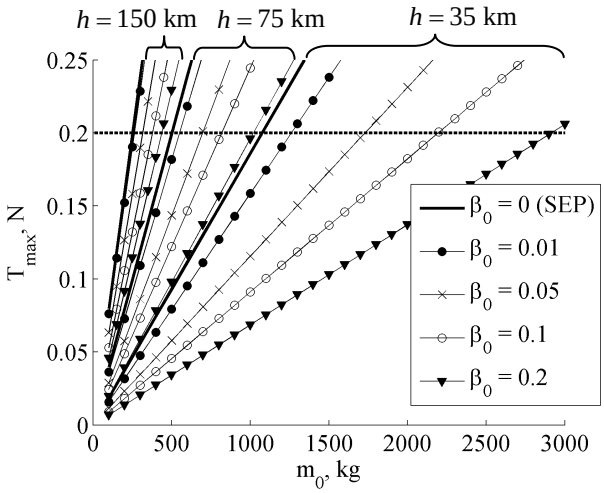

Fig. 15 Maximum thrust magnitude $T_{\max}$ as a function of the initial mass m_0 for different values of the out-of-plane displacement distance h and the sail lightness number β_0 and for $I_{sp} = 3200$ s.

The figure shows that for SEP control and a maximum thrust magnitude of $T_{\max} = 0.2$ N (see Section IV.A), maximum initial masses of 1074, 501 and 251 kg are possible for displacement distances of 35, 75 and 150 km, respectively. These initial masses increase by a factor 1.05 to 2.7 for hybrid sail control, depending on the sail

lightness number and the displacement distance. These higher initial masses show another major advantage of hybrid sail control over SEP control in addition to the propellant mass savings shown in Fig. 7 and Fig. 12.

Using these initial masses and a specific impulse of 3200 s, the payload masses and lifetimes as depicted in Fig. 16 can be obtained. Fig. 16 shows that in almost all cases hybrid sail control outperforms SEP control. The only exception occurs for the largest displacement considered in combination with the largest value for the sail lightness number, $\beta_0 = 0.2$. Fig. 16 furthermore shows that only hybrid sail control allows lifetimes equal to the lifetime of current geostationary spacecraft of 10 - 15 years, while still enabling a considerable payload to be taken onboard. For example, for a 35 km out-of-plane displaced orbit, a sail lightness number of 0.1 and an initial mass of 2193 kg, payload masses of 487 kg and 255 kg can be maintained in the displaced GEO for 10 and 15 years, respectively.

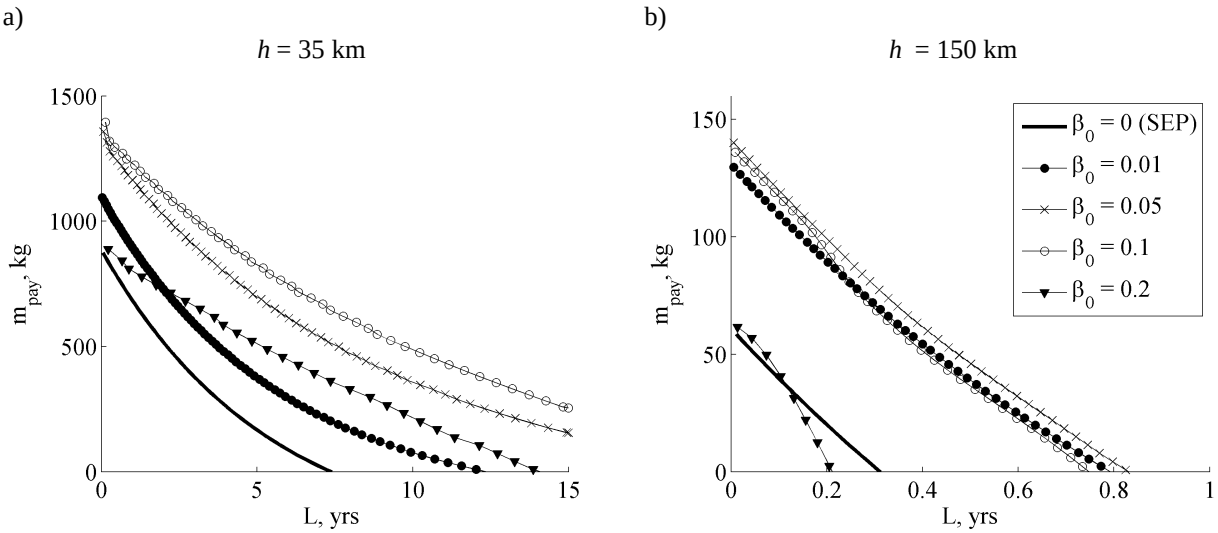

Fig. 16 Payload mass m_{pay} as a function of the mission lifetime L for a 35 km (a) and 150 km (b) out-of-plane displaced GEO, for different sail lightness numbers β_0 and for I_{sp} = 3200 s.

The results in Fig. 16 furthermore suggest that an optimum lightness number exists. For instance, for the 35 km displaced GEO in Fig. 16a the results for $\beta_0 = 0.1$ outperform the results for both smaller and larger values for β_0. Some details on this optimum lightness number are provided in Fig. 17. This figure shows the increase in sail mass and the gain in initial, propellant, tank and power source mass that are achieved by increasing the value for β_0 for a 35 km out-of-plane displaced GEO. The difference between the two lines is thus the net increase in payload mass. The figure clearly shows that for increasing β_0 beyond a certain value, the gain in initial, propellant, tank and power

source mass no longer outweighs the required increased sail mass and increasing β_0 even further would only result in a net decrease of the payload mass. The figure furthermore shows that the optimum value for β_0 depends on the mission lifetime, which is introduced through the dependency of m_{prop} and m_{tank} on both the mission lifetime and the sail lightness number. Note that m_{SEP} and m_{gimbal} are independent of the lightness number and mission lifetime and are therefore of no influence on the graphs in Fig. 17.

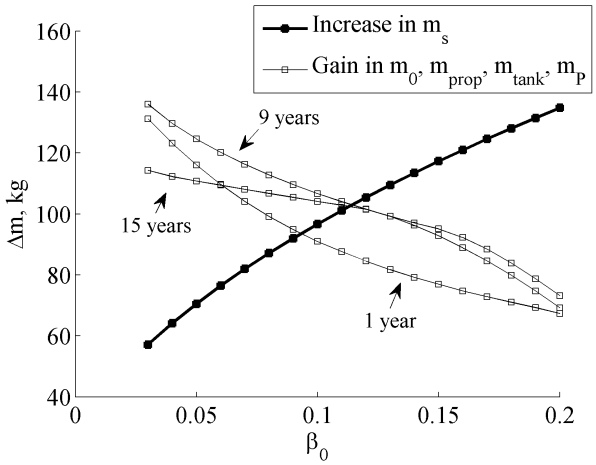

Fig. 17 Increase in sail mass and gain in initial, propellant, tank and power source mass due to increase in sail lightness number β_0 for a 35 km out-of-plane displaced GEO.

Note that the analysis in this section assumes the use of one SEP thruster. However, multiple SEP thrusters could be clustered to provide a larger maximum thrust and with that a larger initial mass. Inspecting the separate mass components in Eq. (41) shows that all components scale linearly with the maximum thrust, including the payload mass. Therefore, by clustering for instance three SEP thrusters to obtain a maximum thrust of 0.6 N, the previously mentioned result for a 35 km out-of-plane displaced orbit and a sail lightness number of 0.1 can be increased to an initial mass of 6579 kg and payload masses of 1461 kg and 765 kg to be maintained in the displaced GEO for 10 and 15 years, respectively.

Although the performance for a 35 km out-of-plane displaced orbit is highly promising, the performance of the higher displaced orbits is not, see Fig. 16b. The lifetime decreases drastically to approximately 0.5 year. Despite this short lifetime an interesting application exists for the 150 km out-of-plane displaced GEO, namely to provide temporary displacements. Then, the displaced GEO is only maintained for a relatively short period of time to provide services when needed and is transferred into a Keplerian parking orbit when inoperative to save propellant mass. For

such short durations, the 150 km displaced GEO can transform its rather short lifetime into multiple smaller mission segments extended over a much longer lifetime. To show the feasibility of this concept, the next section will investigate the trajectory that is required to transfer the spacecraft from and to the Keplerian parking orbit.

VI. Transfer orbits

In the previous section, two types of transfers were mentioned to improve the performance of hybrid sail control for maintaining the out-of-plane displaced GEO. This section will investigate these transfers. Both types of transfers are assumed to be performed using only the onboard SEP system and will be optimized for the propellant consumption. This implies solving an optimal control problem for which the cost function to be minimized is set to:

$$J = -m_f \tag{45}$$

To solve the optimal control problem the open source tool PSOPT is used [40-41]. PSOPT implements a direct pseudospectral method to solve the optimal control problem. By discretizing the time interval into a finite number of nodes, the infinite dimensional optimal control problem is transformed into a finite dimension non-linear programming (NLP) problem. Pseudospectral methods use Legendre or Chebyshev polynomials to approximate and interpolate the time dependent variables at the nodes. The advantage of using pseudospectral methods is that the derivatives of the state functions at the nodes are computed by matrix multiplication only and that any integral associated with the problem is approximated using well known Gauss quadrature rules.

A. Seasonal transfer

The obliquity of the ecliptic causes hybrid sail control for out-of-plane displaced GEOs to perform best when a spacecraft is displaced *above* the equatorial plane (north) in winter and *below* the equatorial plane (south) in summer. To accomplish this, the spacecraft will have to be transferred from above the equatorial plane to below the equatorial plane and vice versa twice per year: once in spring (north to south) and once in autumn (south to north). This seasonal transfer is described using a spherical reference frame $C(r,\theta,\phi)$ centered at the Earth, see Fig. 18. The in-plane angle θ is measured in counter clockwise direction from the x_C axis that coincides with the start of the transfer (i.e. for $t=0$, $\theta=0$) and the out-of-plane angle ϕ is measured from the (x_C, y_C) plane that is parallel to the equatorial plane.

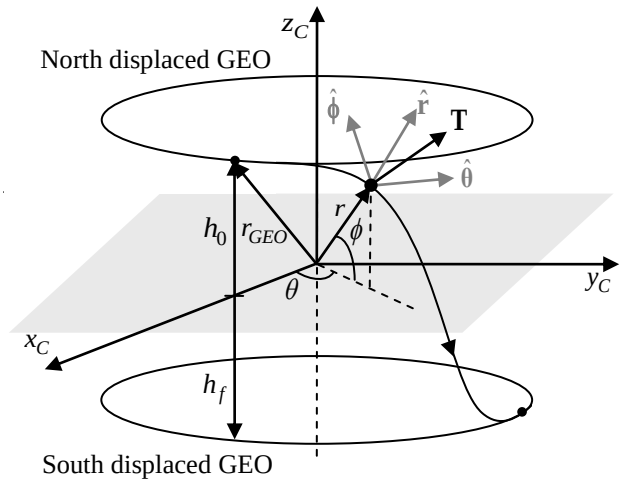

Fig. 18 Definition of spherical reference frame and control vector to describe the seasonal transfer.

For an SEP controlled spacecraft the state vector at any point in the trajectory then becomes:

$$\mathbf{x} = \begin{bmatrix} r & \theta & \phi & V_r & V_\theta & V_\phi & m \end{bmatrix}^T \tag{46}$$

With the transfer starting and ending in a displaced GEO the initial, $\mathbf{x}_0$, and final, $\mathbf{x}_f$, state vectors are given by:

$$\begin{aligned} \mathbf{x}_0 &= [\, r_{GEO} \quad 0 \quad \phi_0 \quad 0 \quad \sqrt{\mu / r_{GEO}} \cos\phi_0 \quad 0 \quad m_0 \,]^T \\ \mathbf{x}_f &= [\, r_{GEO} \quad \theta_f \quad \phi_f \quad 0 \quad \sqrt{\mu / r_{GEO}} \cos\phi_f \quad 0 \quad - \,]^T \end{aligned} \tag{47}$$

with the final mass free. To ensure that the longitude of the spacecraft in the displaced GEO is unchanged after the transfer, the final in-plane angle θ_f is restricted to:

$$\theta_f = \omega_{GEO} t_f \tag{48}$$

Finally, $\phi_0 = \sin^{-1}(h_0 / r_{GEO})$ and $\phi_f = \sin^{-1}(h_f / r_{GEO})$, where correct signs for h_0 and h_f will ensure correct signs for ϕ_0 and ϕ_f.

Using a two-body model, the equations that describe the motion of the spacecraft in the transfer equal:

$$\dot{\mathbf{x}} = \begin{pmatrix} V_r \\ V_\theta / (r \cos\phi) \\ V_\phi / r \\ V_\theta^2 / r + V_\phi^2 / r - \mu / r^2 + T_r / m \\ -V_r V_\theta / r + V_\theta V_\phi \tan\phi / r + T_\theta / m \\ -V_r V_\phi / r - V_\theta^2 \tan\phi / r + T_\phi / m \\ -T / (I_{sp} g_0) \end{pmatrix} \tag{49}$$

with $\mathbf{u} = \begin{bmatrix} T_r & T_\theta & T_\phi \end{bmatrix}$ the control vector consisting of the Cartesian components of the SEP thrust magnitude. This requires the following path constraint:

$$T = \sqrt{T_r^2 + T_\theta^2 + T_\phi^2} \leq T_{\max} \tag{50}$$

with $T_{\max}$ the maximum allowable SEP thrust magnitude.

PSOPT requires an initial guess to initialize the optimization. To obtain this initial guess, a shaped based approach is used in which the shape of the transfer is fixed and the required controls to perform that transfer are sought for. For this, the transfer is considered in a rotating reference frame that rotates with respect to an inertial frame at constant angular velocity equal to the angular velocity of the (displaced) GEO. Within this rotating frame, spacecraft in the north and south displaced GEOs are stationary. Subsequently, the transfer between the orbits is assumed to be the shortest path possible in this reference frame and a parabolic velocity profile is adopted to ensure zero velocities at the start and end of the transfer.

The results of the optimization in PSOPT are given in the first row (for $\Delta d = 0$) of Table 2 with a selection of the corresponding thrust profiles in Fig. 19. A maximum transfer time of one day is assumed to limit a potential disruption in the downlink to Earth during the transfer. Furthermore, to consider the worst case scenario, the maximum masses (i.e. for $\beta_0 = 0.2$) corresponding to a maximum in-orbit thrust magnitude of 0.2 N as shown in Fig. 15 are used for the initial mass m_0. Finally, $T_{\max}$ is set to 0.2 N and a specific impulse of 3200 s is employed. The table shows a relatively worse performance for smaller displacements which can be explained by the relatively larger initial mass. The first row in Table 2 furthermore shows that almost negligible amounts of propellant are needed to perform the seasonal transfer.

Table 2 Required propellant mass in grams for optimized seasonal transfer including a constraint on the approach distance to the GEO, Δd .

		h_0, km		
		±35	±75	±150
m_0, kg		2912	1020	436
Δd , km	0	2.6	0.96	0.66
	5	243.0	52.6	20.1
	10	Infeasible	123.3	42.1
	20	Infeasible	Infeasible	96.0
	35	Infeasible	Infeasible	227.4

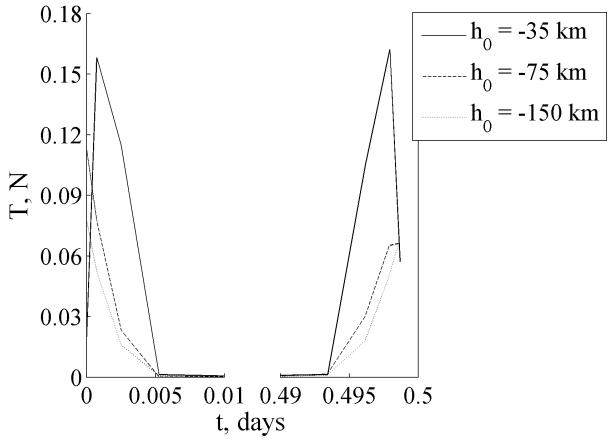

Fig. 19 Thrust profile for optimized seasonal transfer with $\Delta d = 0$.

The reason for these small amounts of propellant can be found when considering what happens when the propulsion is switched off in the displaced GEO. The spacecraft will fall into a Keplerian orbit for which the inclination is equal to ϕ, the eccentricity is close 0 and the semi-major axis is close to the GEO radius [2]. The Keplerian orbit thus almost coincides with the displaced GEO on the opposite side of the equatorial plane and only a small thrust is needed to overcome any remaining offset. This description of the transfer also implies that the transfer closely passes the GEO and could therefore impose collision risk to GEO spacecraft. In order to cope with this, the following path constraint is added to the optimal control problem:

$$\sqrt{r_{GEO}^2 - 2r \cdot r_{GEO} \cos\phi + r^2} \geq \Delta d \tag{51}$$

which ensures that the distance between the transfer and the GEO is always larger than the value assigned to Δd. Including this constraint provides the other results in Table 2, where the propellant mass is given for different values of Δd. The table shows that the constraint has a rather large impact on the propellant consumption, especially for the smaller displacements. However, the increase in propellant mass still outweighs the savings that can be obtained from applying the transfer to increase the performance of the out-of-plane displaced GEO during the in-orbit phase.

B. Temporary displacement

For the temporary displacement, the spacecraft is transferred into an out-of-plane displaced GEO for a relatively short period of time to provide services and is transferred back into a Keplerian parking orbit when the services are no longer needed in order to save propellant mass. This parking orbit and the transfer that are involved in this concept are illustrated in Fig. 20. The parking orbit thus lies in the equatorial plane and inside the GEO, where the

distance between the parking orbit and the GEO equals the absolute value of the displacement distance. In this way, the parking orbit is as close to the displaced GEO as possible without interfering with either the GEO or the displaced GEO.

The investigation of the transfer between the parking orbit and the displaced GEO (and vice versa) is very similar to the seasonal transfer. The definition of the state and control variables is the same as are the equations of motion. Only the initial and final states differ. When the transfer from the parking orbit to the displaced GEO is considered, these become:

$$\mathbf{x}_0 = [r_{GEO} - |h| \quad 0 \quad 0 \quad 0 \quad \sqrt{\mu/(r_{GEO} - |h|)} \quad 0 \quad m_0]^T \tag{52}$$

$$\mathbf{x}_f = [r_{GEO} \quad - \quad \phi_f \quad 0 \quad \sqrt{\mu/r_{GEO}}\cos\phi_f \quad 0 \quad - \quad]^T \tag{53}$$

with the final mass and final in-plane angle free. Phasing between the parking orbit and the out-of-plane displaced GEO will have to ensure that the spacecraft is inserted into the displaced GEO at the correct longitude. Note that when the transfer from the displaced orbit to the parking orbit is considered, the initial condition equals Eq. (53) and the final condition becomes Eq. (52).

In addition to the problem definition, also the optimization of the transfer is similar to the optimization of the seasonal transfer. The same method to generate the initial guess and the same objective function and path constraints can be applied. The results of the optimization are shown in Table 3 and Fig. 21, where again a minimum distance from the GEO is taken into account. Although the required propellant mass is larger than for the seasonal transfer, it still requires only modest propellant budgets, and improvements could possibly be made by employing the solar sail in case hybrid sail control is used to maintain the out-of-plane displaced GEO.

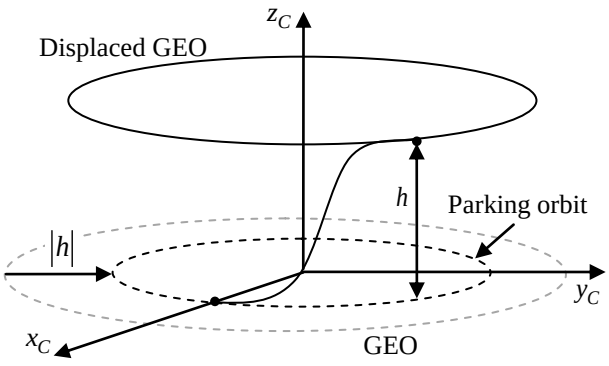

Fig. 20 Definition of parking orbit for temporary displacement.

Table 3 Required propellant mass in grams for temporary displacement transfer including a constraint on the approach distance to the GEO, Δd .

		Parking orbit to displaced GEO			Displaced GEO to parking orbit		
		h_f , km			h_0 , km		
		±35	±75	±150	±35	±75	±150
m_0 , kg		2912	1020	436	2912	1020	436
Δd , km	0	277.8	204.0	173.7	292.0	208.9	176.1
	5	287.2	206.7	174.1	297.3	209.9	176.2
	10	302.3	210.9	176.1	304.3	214.1	177.3
	20	Infeasible	221.4	179.5	Infeasible	224.6	181.1
	35	Infeasible	247.2	185.7	Infeasible	249.9	187.2

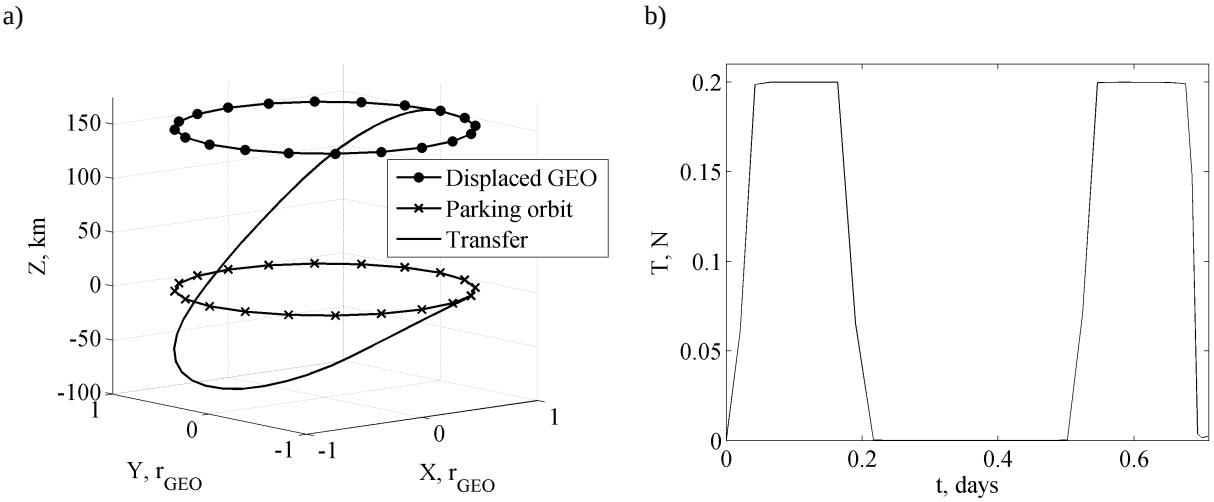

Fig. 21 a) Temporary displacement transfer from a 150 km out-of-plane displaced GEO. b) Thrust profile.

VII. Conclusions

In this paper displaced geostationary orbits (GEOs) have been proposed to increase the capacity of the GEO at longitude slots where it is starting to become congested. By levitating the GEO above or below the equatorial plane or by displacing it in the equatorial plane, new slots arise, but at the cost of a continuously required control. Three types of control have been suggested: impulsive, solar electric propulsion (SEP) and hybrid sail control. For all three types of control it was shown that, for similar displacements, the out-of-plane displaced GEO outperforms the in-plane displaced GEO in terms of ΔV or required SEP acceleration and with that in terms of propellant mass or mission lifetime. Due to a penalty on the ΔV for using pulsed rather than continuous control to maintain an out-of-

plane displaced GEO and the low specific impulse of a chemical propulsion system, the performance of impulsive control was found to be very poor. Even small displacements of 35 km, the minimum to rise above the geostationary station keeping box, could not be maintained for longer than a few months. Much better performance of a few months to a few years in a 150 km and 35 km out-of-plane displaced orbit, respectively, could be observed for the use of SEP control. However, investigating the spacecraft mass budget showed that only for small displacements reasonable payload masses of a few hundred kilograms could be maintained for a few years. By adding a solar sail to the SEP system, thereby creating hybrid sail control, the demand on the SEP system could be lowered while enabling a mission that is impossible using only a solar sail due to the obliquity of the ecliptic and the inability of the sail to produce a thrust force in the direction of the Sun. The hybrid control case has been optimized for the SEP propellant consumption, thereby maximizing the mission lifetime and payload mass. A seasonal transfer could be performed between orbits displaced above and below the equatorial plane to maximize the sail's performance and further optimize these results. Optimizing this transfer for the SEP propellant consumption showed that this transfer comes almost for free or at the cost of a modest propellant budget, depending on the allowed approach distance to the GEO. Employing the seasonal transfer provided lifetimes of 10 - 15 years (equal to current geostationary missions) for a 35 km out-of-plane displaced orbit and for considerable payload masses of 255 - 487 kg, assuming the use of one SEP thruster. These payload masses could be increased linearly by increasing the number of SEP thrusters. The higher out-of-plane displaced orbits appeared to be especially useful for temporary displacements in which the spacecraft is only put into the displaced orbit for relatively short periods of time to provide coverage when needed. When not operational, the spacecraft is transferred into a Keplerian parking orbit to save propellant mass. Optimizing this transfer showed that again only a modest propellant budget is required.

Acknowledgments

This work was funded by the European Research Council Advanced Investigator Grant - 227571: Visionary Space Systems: Orbital Dynamics at Extremes of Spacecraft Length-Scale. The authors would like to thank Victor M. Becerra of the University of Reading for providing the software tool PSOPT freely and providing advice on its use.

References

1. Jehn, R., Rossi, A., Flohrer, T., Navarro-Reyes, D., "Reorbiting of Satellites in High Altitudes", *5th European Conference on Space Debris*, Darmstadt, Germany, 30 March-2 April, 2009.

2. McInnes, C. R., "*Solar Sailing: Technology, Dynamics and Mission Applications*", Springer-Praxis Books in Astronautical Engineering, Springer-Verlag, Berlin, 1999. p. 1-2, 40, 171-228.

3. McInnes, C. R., "Dynamics, Stability, and Control of Displaced Non-Keplerian Orbits", *Journal of Guidance, Control, and Dynamics*, vol. 21, n. 5, p. 799-805, 1998. doi: 10.2514/2.4309

4. Biggs, J. D., McInnes, C. R., Waters, T., "Control of Solar Sail Periodic Orbits in the Elliptic Three-Body Problem", *Journal of Guidance, Control, and Dynamics*, vol. 32, n. 1, p. 318-320, 2009. doi: 10.2514/1.38362

5. McKay, R. J., Macdonald, M., Biggs, J., McInnes, C., "Highly Non-Keplerian Orbits with Low-Thrust Propulsion", *Journal of Guidance, Control, and Dynamics*, vol. 34, n. 3, 2011.

6. McInnes, C. R., "The Existence and Stability of Families of Displaced Two-Body Orbits", *Celestial Mechanics and Dynamical Astronomy*, vol. 67, p. 167-180, 1997. doi: 10.1023/A:1008280609889

7. Waters, T. J., McInnes, C. R., "Periodic Orbits above the Ecliptic in the Solar-Sail Restricted Three-Body Problem", *Journal of Guidance, Control, and Dynamics*, vol. 30, n. 3, p. 687-693, 2007. doi: 10.2514/1.26232

8. Simo, J., McInnes, C. R., "Solar Sail Orbits at the Earth-Moon Libration Points", *Communications in Nonlinear Science and Numerical Simulation*, vol. 14, n. 12, p. 4191-4196, 2009. doi: 10.1016/j.cnsns.2009.03.032

9. Grebow, D. J., Ozimek, M. T., Howell, K. C., "Advanced Modeling of Optimal Low-Thrust Lunar Pole-Sitter Trajectories", *Acta Astronautica*, vol. 67, p. 991-1001, 2010. doi: 10.1016/j.actaastro.2010.04.024

10. Baig, S., McInnes, C. R., "Light-Levitated Geostationary Cylindrical Orbits Are Feasible", *Journal of Guidance, Control, and Dynamics*, vol. 33, n. 3, p. 782-793, 2010. doi: 10.2514/1.46681

11. JAXA, "Press Releases: Small Solar Power Sail Demonstrator 'Ikaros' Confirmation of Photon Acceleration", available from: http://www.jaxa.jp/press/2010/07/20100709_ikaros_e.html, cited 1 September 2010

12. Newton, K., "Nasa's First Solar Sail Nano Sail-D Deploys in Low-Earth Orbit", available from: http://www.nasa.gov/centers/marshall/news/news/releases/2011/11-010.html, cited 24 January 2011

13. Macdonald, M., McInnes, C. R., "Solar Sail Mission Applications and Future Advancement", *2nd International Symposium on Solar Sailing (ISSS 2010)*, New York, USA, 20-22 July, 2010.

14. McKay, R., Macdonald, M., Bosquillon de Frescheville, F., Vasile, M., McInnes, C., Biggs, J., "Non-Keplerian Orbits Using Low Thrust, High Isp Propulsion Systems", *60th International Astronautical Congress*, IAC-09.C1.2.8, Daejeon, South Korea, 12-16 October, 2009.

15. Mengali, G., Quarta, A. A., "Trajectory Design with Hybrid Low-Thrust Propulsion System", *Journal of Guidance, Control, and Dynamics*, vol. 30, n. 2, p. 419-426, 2007. doi: 10.2514/1.22433

16. Mengali, G., Quarta, A. A., "Tradeoff Performance of Hybrid Low-Thrust Propulsion System", *Journal of Spacecraft and Rockets*, vol. 44, n. 6, p. 1263-1270, 2007. doi: 10.2514/1.30298

17. Simo, J., McInnes, C. R., "Designing Displaced Lunar Orbits Using Low-Thrust Propulsion", *Journal of Guidance, Control, and Dynamics*, vol. 33, n. 1, p. 259-265, 2010. doi: 10.2514/1.45305

18. Baig, S., McInnes, C. R., "Artificial Three-Body Equilibria for Hybrid Low-Thrust Propulsion", *Journal of Guidance, Control, and Dynamics*, vol. 31, n. 6, p. 1644-1655, 2008. doi: 10.2514/1.36125

19. McKay, R. J., Macdonald, M., Vasile, M., Bosquillon de Frescheville, F., "A Novel Interplanetary Communications Relay", *AIAA/AAS Astrodynamics Specialist Conference*, AIAA-2010-7964, Toronto, Canada, 2-5 August, 2010.

20. Ceriotti, M., McInnes, C. R., "Generation of Optimal Trajectories for Earth Hybrid Pole-Sitters", *Journal of Guidance, Control, and Dynamics*, vol. 34, n. 3, 2011.

21. Heiligers, J., "Displaced Geostationary Orbits Using Hybrid Low-Thrust Propulsion", *61st International Astronautical Congress*, Prague, Czech Republic, 27 September - 1 October, 2010.

22. Forward, R. L., "Light-Levitated Geostationary Cylindrical Orbits Using Perforated Light Sails", *Journal of the Astronautical Sciences*, vol. 32, p. 221-226, 1984.

23. Meserve, B. E., "*Fundamental Concepts of Algebra*", Dover Publications, New York, 1982. p. 156-159.

24. Vallado, D. A., "*Fundamentals of Astrodynamics and Applications*", 3rd Edition, Space Technology Library, New York, USA, 2007. p. 72-73, 389-398.

25. Evans, B. G., "*Satellite Communication Systems*", 3rd Edition, The Institution of Engineering and Technology, London, UK, 1999. p. 272.

26. UNCOPUOS, "Long-Term Sustainability of Outer Space Activities, Preliminary Reflections", *47th session of the United Nations Committee on the Peaceful Uses of Outer Space (UNCOPUOS) Scientific and Technical Subcommittee*, Vienna, Austria, 8-19 February, 2010.

27. Spilker, T. R., "Saturn Ring Observer", *Acta Astronautica*, vol. 52, p. 259-265, 2003. doi: 10.1016/S0094-5765(02)00165-0

28. Yashko, G. J., Hastings, D. E., "Analysis of Thruster Requirements and Capabilities for Local Satellite Clusters", *AIAA Small Satellite Conference*, Logan, USA, 16-19 September, 1996.

29. Wertz, J. R., Larson, W. J., "*Space Mission Analysis and Design*", 3rd Edition, *Space Technology Series*, Space Technology Library, Microcosm Press/Kluwer Academic Publishers, El Segundo, USA/London, UK, 1999. p. 333, 412, 692, 703.

30. Kuninaka, H., Nishiyama, K., Funaki, I., Yamada, T., Shimizu, Y., Kawaguchi, J., "Powered Flight of Electron Cyclotron Resonance Ion Engines on Hayabusa Explorer", *Journal of Propulsion and Power*, vol. 23, n. 3, 2007.

31. Schneider, A., Sun, W., Schuff, H., "The European Platform Luxor for Small Communications Satellites", *26th International Communications Satellite Systems Conference (ICSSC)*, AIAA-2008-5441, San Diego, USA, 10-12 June, 2008.

32. Dachwald, B., Mengali, G., Quarta, A. A., Macdonald, M., "Parametric Model and Optimal Control of Solar Sails with Optical Degradation", *Journal of Guidance, Control, and Dynamics*, vol. 29, n. 5, p. 1170-1178, 2006. doi: 10.2514/1.20313

33. Powell, M., "A Fast Algorithm for Nonlinearly Constrained Optimization Calculations", in *Numerical Analysis*, G. Watson, Editor. 1978, Springer Berlin / Heidelberg. p. 144-157. doi: 10.1007/BFb0067703

34. Ceriotti, M., McInnes, C. R., "Systems Design of a Hybrid Sail Pole-Sitter", *Advances in Space Research*, in press, 2011. doi: 10.1016/j.asr.2011.02.010

35. Gershman, R., Seybold, C., "Propulsion Trades for Space Science Missions", *Acta Astronautica*, vol. 45, p. 541-548, 1999. doi: 10.1016/S0094-5765(99)00174-5

36. Kitamura, S., Ohkawa, Y., Hayakawa, Y., Yoshida, H., Miyazaki, K., "Overview and Research Status of the Jaxa 150-Mn Ion Engine", *Acta Astronautica*, vol. 61, p. 360-366, 2007. doi: 10.1016/j.actaastro.2007.01.010

37. Leipold, M., Götz, M., "Hybrid Photonic/Electric Propulsion". Kayser-Threde GmbH, 2002.

38. Murphy, D. M., Murphey, T. W., Gierow, P. A., "Scalable Solar-Sail Subsystem Design Considerations", *43rd Structures, Structural Dynamics, and Materials Conference*, AIAA-2002-1703, Denver, USA, 22-25 April, 2002.

39. Dachwald, B., "Optimal Solar Sail Trajectories for Missions to the Outer Solar System", *AIAA/AAS Astrodynamics Specialist Conference and Exhibit*, AIAA-2004-5406, Providence, USA, 16 - 19 August, 2004.

40. Becerra, V. M., "Psopt Optimal Control Solver User Manual", available from: http://www.psopt.org/, cited 1 October 2010

41. Becerra, V. M., "Solving Complex Optimal Control Problems at No Cost with Psopt", in *Proceedings of IEEE Multi-conference on Systems and Control*, Yokohama, Japan, 2010.